Variability and extremes: Statistical validation of the AWI-ESM

Justus Contzen[1,2], Thorsten Dickhaus[3], and Gerrit Lohmann[1,2]

[1]Alfred Wegener Institute Helmholtz Centre for Polar and Marine Research, Bremerhaven, Germany
[2]Department of Environmental Physics, University of Bremen, Bremen, Germany
[3]Institute for Statistics, University of Bremen, Bremen, Germany

Correspondence: Justus Contzen (justus.contzen@awi.de)

Abstract. Coupled general circulation models are of paramount importance to assess quantitatively the magnitude of future climate change. Usual methods for validating climate models include the evaluation of mean values and covariances, but less attention is directed to the evaluation of extremal behaviour. This is a problem because many severe consequences of climate changes are due to climate extremes. We present a method for model validation in terms of extreme values based on classical extreme value theory. We further discuss a clustering algorithm to detect ~~spacial~~ spatial dependencies and tendencies for concurrent extremes. To illustrate these methods, we analyse precipitation extremes of the AWI-ESM global climate model ~~compared~~ as well as of other models that take part in the Coupled Model Intercomparison Project CMIP6 and compare them to the reanalysis data set CRU TS4.04. The ~~methods~~ clustering algorithm presented here can ~~also be used for the comparison of model ensembles~~ be used to determine regions of the climate system that are then subjected to a further in-depth analysis, and there may ~~be further~~ also be applications in palaeoclimatology.

1 Introduction

Coupled general circulation models are frequently utilised to assess quantitatively the magnitude of future climate change. Validating these models by simulating different climate states is essential for understanding the sensitivity of the climate system to both natural and anthropogenic forcing. Usual methods for validating climate models include the evaluation of mean values and covariances and the comparison of empirical cumulative distribution functions. These analyses can also be conducted over seasonal and annual averages (climatologies) or along latitudinal/longitudinal transects (Tapiador et al., 2012). The comparison of climate indices is also common in model validation (Sillmann et al., 2013; Zhang et al., 2011). While climate models are able to reproduce many climate phenomena across the globe, their reliability regarding extremes requires additional evaluation. Changes in the intensity and frequency of extremes have drawn much attention during recent decades (IPCC, 2012; Rahmstorf and Coumou, 2011; Horton et al., 2016), mainly due to their large impacts on natural environment, economy and human health (Ciais et al., 2005; Kovats and Kristie, 2006). For instance, the summer heat wave over Central Europe in 2003 resulted in extensive forest fires, crop yield reductions and fatalities (de Bono et al., 2004; Vandentorren et al., 2004). During the 20th century, the frequency of high-temperature extremes has increased in Europe (Dong et al., 2017), even after the apparent levelling off of global mean temperatures after 2000 (Trenberth and Fasullo, 2013), and for precipitation extremes, a similar development has been observed (Fischer and Knutti, 2016). Due to the inherent nature of extreme events,

their evolution differs from that of the mean and the variance (Schär et al., 2004; IPCC, 2012) and also ~~highly~~ depends on the strength of the events themselves (Myhre et al., 2019).

In particular, the concurrent occurrence of climate extremes at different locations may have especially large impacts on agriculture (Toreti et al., 2019), human societies and economies (Jongman et al., 2014) and on the climate system itself (Zscheischler et al., 2014). Large-scale climate extremes can furthermore cause serious problems for insurance and reinsurance companies (Mills, 2005). For these reasons, an increasing amount of research is being conducted on multivariate analysis of extremes with focus on their concurrent appearance (Shaby and Reich, 2012; Dombry et al., 2018; Kornhuber et al., 2020; Ionita et al., 2021a) and new tools have been created for the analysis of extremes in climate models (Weigel et al., 2021).

~~The~~ A particular challenge for the analysis of extreme events is ~~often complicated by~~ the fact that extreme events are typically rare, and that it is therefore difficult to build informative statistics based solely on the extreme events themselves. ~~As a remedy, it is common to apply the~~ Two common approaches are used to overcome this issue: peaks-over-threshold and block-maxima ~~approach, i. e. to group data~~. In the peaks-over-threshold approach, a fixed threshold is selected. The distribution of the data exceeding this threshold can then be approximated by a generalised Pareto distribution if some additional assumptions are fulfilled (see McNeil et al. (2015), Chapter 7.2 for more details). The peaks-over-threshold approach is frequently applied in climatology and hydrology (Acero et al., 2011; Fowler and Kilsby, 2003; Kiriliouk et al., 2019). The block-maxima approach, on the other hand, follows the idea to split the time axis into blocks of a sufficiently large size and investigate the block-wise maxima of the data. Under suitable conditions, the distribution of these block-wise maxima can ~~be described with the~~ for large sample sizes be approximated by a generalised extreme value (GEV) distribution.

In this work, we will evaluate the performance of the fully coupled ~~AWI Earth~~ Alfred Wegener Institute-Earth System Model AWI-ESM1.1LR (Shi et al., 2020; Lohmann et al., 2020; Ackermann et al., 2020) in terms of its accuracy regarding variability and extremes of precipitation, putting special focus on spatially concurrent precipitation extremes. Our main questions are whether the model is able to ~~correctly~~ accurately reproduce extreme events in different regions and ~~if~~ whether spatial dependencies and concurrent extremal events are ~~correctly identified~~ modelled adequately. We compare model data from a historical run of the AWI-ESM to the global precipitation reanalysis data set CRU TS4.04 (Harris et al., 2020). We start with investigating variability and extremes locally using empirical ~~statistics~~ statistical parameters and by fitting a GEV distribution to annual precipitation maxima. Then, following an approach by Bernard et al. (2013), we use a clustering algorithm to group spatio-temporal climate data into different spatial regions based on their similarity in terms of extremal behaviour and the concurrency of their extremes. This clustering is based on the theory of max-stable copulae, which has been used ~~extensively~~ in prior work to investigate spatial dependence of extreme precipitation events, for example in Bargaoui and Bárdossy (2015); Zhang et al. (2013); Qian et al. (2018). In those papers, an analysis of bivariate ~~variables~~ distributions is performed. In our work, we first construct for each pair of locations a measure for their ~~similary~~ similarity in terms of extremes. This measure is then used as a basis for the clustering algorithm to group the data into spatial regions of comparable extremal behaviour.

The resulting clusters for model and observational data are compared and used to analyse the ability of the climate model to ~~correctly~~ reproduce spatial dependencies of precipitation extremes.

~~Applying clustering algorithms to climate data is~~ In this article, our main focus is on the AWI-ESM and we present our methods using data from this model. We also present a measure for the model accuracy in regard to extremal precipitation, and apply it to a set of different CMIP6 models. In the main text, results will be discussed for the AWI-ESM and for the model identified as having the best model accuracy. In the supplement to this paper, the results for the other CMIP6 models investigated are presented.

Model validation in terms of precipitation extremes is already an active research topic. Tabari et al. (2016) investigate the performance of global and regional climate models using the peaks-over-threshold approach. An evaluation of regional and global climate models using extreme precipitation indices is conducted by Bador et al. (2020a), revealing a tendency for stronger extremes in regional models. A similar result was obtained by Mahajan et al. (2015) by comparing climate model and observational precipitation data over the United States using GEV distributions. Timmermans et al. (2019) conduct pairwise comparisons of the precipitation extremes of numerous gridded observation-based datasets and find considerable differences between the datasets especially in mountainous regions. Precipitation extremes over India are investigated by Mishra et al. (2014) using GEV distributions and comparisons of indices with a focus on changes over time.

It is also not a new approach to apply clustering algorithms to climate data. Among others, it has been used to define climate zones in the United States (Fovell and Fovell, 1993) and globally (Zscheischler et al., 2012), and to find regions with similar trends in their climatic change over Europe (Carvalho et al., 2016). Those analyses focus on mean values and on their temporal differences, respectively, while we apply clustering specifically to uncover connections regarding climate extremes.

The article is structured as follows: After introducing the data sets in Sect. 2, we present the methods used in Sect. 3. The results from their application to the data are presented in Sect. 4. A section on conclusions and discussions finalises the article.

2 Data

The observational data are reanalysed monthly precipitation data in mm over land (excluding Antarctica) from the CRU TS4.04 data set (Harris et al., 2020; University of East Anglia Climatic Research Unit et al., 2020) with data ranging from 1901 to 2019. We restrict the time frame to the years 1930 to 2014 in order to have a sufficiently large area with non-missing data and to be consistent with the climate model data. The grid size is $0.5° \times 0.5°$, the data have been obtained by interpolating observations from more than 4.000 weather stations using angular distance weighting.

At some locations and time points, no data from nearby weather stations ~~was~~ had been available to use for interpolation. In these cases, the creators of the CRU TS4.04 data set used a value from a climatology instead. These climatology values are

~~uninformative~~ not very informative in terms of extremes and too many of them would distort the analyses, therefore all grid points with more than 5% climatology values and additionally all grid points with at least ~~12~~ twelve consecutive months of climatology values are excluded from our analysis. This results in the exclusions of larger regions in northern and central Africa, in Indonesia, in central Asia and in the polar regions. In the figures ~~below~~showing geographical data in this paper, those regions are coloured in grey.

The climate model used is the coupled model AWI-ESM1.1LR. It is based on the AWI Earth System Model (AWI-ESM1), which consists of the AWI Climate Model (Sidorenko et al., 2015; Rackow et al., 2018), but with interactive vegetation. The model comprises the atmosphere model ECHAM6 (Stevens et al., 2013), which is run with the T63L47 setup ~~,~~(that is, a horizontal resolution of $1.85° \times 1.85°$ ~~. The~~ and 47 vertical layers) and the ocean-sea ice model FESOM1.4 (Wang et al., 2014), which employs an unstructured grid, allowing for varying resolutions from 20km around Greenland and in the North Atlantic to around 150km in the open ocean (CORE2 mesh). The land surface processes are computed by the land surface model JSBACH2.11 (Reick et al., 2013). The model considers the surface runoff toward the coasts, deploying a hydrological discharge model that also includes freshwater fluxes by snowmelt (Hagemann and Dümenil, 1997).

AWI-ESM1 has been extensively used and described in the context of palaeoclimate changes as well as of changes of the recent and future climate (Shi et al., 2020; Lohmann et al., 2020; Ackermann et al., 2020; Niu et al., 2021). The historical run is documented in Danek et al. (2020) and has been directly used in Ackermann et al. (2020) and Keeble et al. (2021). The model takes furthermore part in CMIP6/PMIP4 activities (Brierley et al., 2020; Brown et al., 2020; Otto-Bliesner et al., 2021; Kageyama et al., 2021a, b).

The Coupled Model Intercomparison Project CMIP, coordinated by the Working Group on Coupled Modelling (WGCM) of the World Climate Research Programme (WCRP), has the goal to support and facilitate the analysis of climate model data by providing a set of common standards regarding the formatting and availability of model output. Additionally, in order to enhance model comparability, all models participating in CMIP are required to run a set of standardised experimental setups (Diagnostic, Evaluation and Characterization of Klima experiments; DECK experiments) as well as a simulation of the historical climate from 1850 until 2014 (the historical simulations we also use in our analysis). CMIP is divided into different phases reflecting the advancements of climate modelling, the current phase CMIP6 started in 2016. More information on CMIP can be found in Eyring et al. (2016). The model outputs are made available by the Earth System Grid Federation (ESGF; Cinquini et al., 2014).

In our analysis, we restrict the time frame ~~is restricted~~ of the model data to the years 1930 to 2014, as in the observational data. We investigate monthly precipitation (sum of convective precipitation and large-scale precipitation) in mm/month. We use bilinear interpolation to scale the reanalysis data to the ~~$1° \times 1°$~~ grid of the ~~reanalysis data set~~ atmospheric component of the climate model and take into account only those interpolated grid points that correspond to locations with given observed

data, excluding the oceans and the regions with incomplete data mentioned above.

3 Methods

3.1 Univariate Analysis

In this subsection, the time series of ~~all data points are~~ each spatial location (henceforth referred to as grid point) is investigated separately, and all operations and analyses described are therefore conducted for each grid point. Since the focus of this work is not on evaluating the effects of long-time trends, we apply a seasonal-trend decomposition using Loess (Cleveland et al., 1990) on the data and subtract the deviance of the trend from its mean value from it, resulting in data ~~that can be assumed time-stationary~~ for which we assume temporal stationarity. Then, as a first comparison between the data sets, we investigate differences in the empirical mean and empirical standard deviation of the annually maximised precipitation data.

The theoretical foundation for the application of the GEV distribution is as follows: For a random variable X with an unknown probability distribution, we ~~look at~~ investigate the distribution of the maximum of i.i.d. copies $X_1, \ldots, X_n$ of it: $Y^{(n)} := \max_{i=1,\ldots,n}(X_i)$. We assume that for suitable normalising sequences $a_n > 0$ and b_n, ~~these blockwise maxima converge~~ $Y^{(n)}$ converges in distribution if ~~the block size~~ n tends to infinity:

$$\frac{Y^{(n)} - b_n}{a_n} \xrightarrow{\mathcal{D}} H. \tag{1}$$

In this case, as shown by Fréchet (1927), Fisher and Tippett (1928) and Gnedenko (1943), the distribution of $Y^{(n)}$ can be approximated by a GEV distribution for a large (fixed) value of n. This distribution depends on the three parameters location (μ), scale ($\sigma > 0$) and shape (γ) and its cumulative distribution function is given by

$$F_{\mu,\sigma,\gamma}(x) = \begin{cases} \exp(-\exp(-\frac{x-\mu}{\sigma})) & \gamma = 0 \\ \exp(-\max(0, 1+\gamma\frac{x-\mu}{\sigma})^{-\frac{1}{\gamma}}) & \gamma \neq 0. \end{cases} \tag{2}$$

The GEV distribution has widely been used as a model for blockwise maximised data ~~, especially for the yearly maximum of daily average precipitation (Coles et al., 2003; Onwuegbuche et al., 2019; Villarini et al., 2011, for example)~~(for example Coles et al., 2003. Following this approach, we group our monthly precipitation data from observations and climate model into one-year block maxima and fit a GEV distribution to the blockwise maxima at each grid point. When selecting a block size, a bias-variance tradeoff has to be taken into account: For a low block size, the ~~resultung~~ resulting parameter estimates tend to be biased because the convergence to the GEV distribution holds only asymptotically. A high block size, on the other hand, will lead to a limited amount of block-wise maxima that can be analysed and therefore to a higher variance in the estimates (see McNeil et al. (2015), Chapter 7). In our case, we have a relatively small block size of 12 (months per year) and a number of block-wise maxima of 90 (years of investigation).

To estimate the distribution parameters, we use the method of ~~Probability-Weighted Moments~~ probability-weighted moments developed by Hosking (1985) as implemented in the R package "EnvStats" of Millard (2013). As shown by Hosking et al. (1985), this method yields estimators with a relatively low variance and bias compared to the maximum likelihood approach, especially for small and medium-size samples. We test the goodness of fit using a one-sided Kolmogorov-Smirnov-test at ~~significane~~ significance level 5%. The null hypothesis of the test is that the annually maximised data follow the GEV distribution having the probability-weighted moments estimates as distribution parameters.

~~For each parameter, we also compute~~ We also use the parametric bootstrap method with 2500 resamples to compute 95% confidence intervals for each GEV parameter and for the 95% quantiles of the distributions. Confidence intervals for the GEV parameters based on asymptotic normality also exist for the probability-weighted moments estimators, but, as shown by Hosking et al. (1985), they have a high bias and variance if the shape parameter is far away from zero. In our data, for several time series such a value is estimated for the shape parameter, and comparisons between the confidence intervals based on bootstrap and those based on asymptotic normality also confirmed large differences in these cases. For the sake of methodological consistency and because we also use the bootstrap for the confidence intervals of the 95% quantiles, we calculated the GEV parameter confidence intervals using ~~the parametric bootstrap method with 2500 resamples.~~ bootstrap for all time series. Since this method is quite time-consuming, it could also be advocated to choose the method of confidence interval calculation based on the estimated shape parameter value.

To compare the performance of different CMIP6 models, we introduce as a measure for the accuracy of the extremal precipitation an Average Weighted Quantile Difference (AWQD). For this measure, the absolute differences between model and observational 95% GEV quantiles, weighted with the cosine of the latitude, are averaged. The weighting accounts for the fact that the grid cells do not have an equal size for all grid points, and the average is taken because of the different model resolutions. For $\mathcal{G}$ the set of grid points and estimated quantiles $\hat{q}_{0.95,\text{mod}}(g)$ and $\hat{q}_{0.95,\text{obs}}(g)$ for $g \in \mathcal{G}$, we therefore define

$$\text{AWQD} := \frac{1}{|\mathcal{G}|} \sum_{g \in \mathcal{G}} \cos(\text{lat}(g)) \cdot |\hat{q}_{0.95,\text{mod}}(g) - \hat{q}_{0.95,\text{obs}}(g)|. \tag{3}$$

3.2 Comparison of spatial distributions

To compare the spatial distributions of climate extremes, we introduce a hierarchical clustering algorithm (using average linking) to determine regions with similar extremal behaviour. This approach is similar to the idea proposed in Bernard et al. (2013). ~~For hierarchical clustering, an appropriate dissimilarity function $D : A \times A \to \mathbb{R}$ with A the total set of grid points is required. This function must fulfil $D(x,x) = 0$ and $D(x,y) = D(y,x) \geq 0$ for all $x, y \in A$.~~ The hierarchical clustering is based on concepts from extreme value statistics that will be discussed in the following.

~~One possible dissimilarity measure is based on the extremal coefficient $\theta_{x,y}$, a measure of the strength of the dependency of GEV distributed attaining a low value if the extremes in the distributions at x and y tend to be concurrent. The extremal coefficient is based on the theory of max-stable copulae: Assume that the~~

Assume that two real-valued random variables (X, Y) have a copula function $C : [0,1] \times [0,1] \to [0,1]$, that is, their joint distribution function can be written in terms of the copula and the marginal distribution functions as $F_{X,Y}(x,y) = C(F_X(x), F_Y(y))$ for all $x, y \in \mathbb{R}$. Then, if (X, Y) is the weak limit of block-wise maxima of a sequence of i.i.d. two-dimensional variables when the block size goes to infinity (a similar condition as in Sect. 3.1, extended to two-dimensional random variables), it follows that X and Y are (jointly) GEV distributed. It follows as well that the copula must fulfil $C(u^t, v^t) = C^t(u,v)$ for all $u, v \in [0,1]$ and $t > 0$ (see McNeil et al. (2015), Theorem 7.44 and 7.45). Such a copula is called max-stable and it can be written as

$$C(u, v) = \exp\left((\ln u + \ln v) A_{X,Y}\left(\frac{\ln u}{\ln u + \ln v} \right) \right) \tag{4}$$

using a function $A_{X,Y} : [0,1] \to [\tfrac{1}{2}, 1]$ called the Pickands dependence function (Pickands, 1981). The function $A_{X,Y}$ is convex and satisfies $\max(w, 1-w) \le A_{X,Y}(w) \le 1$ for all $w \in [0,1]$. The extremal coefficient is now defined as two times its value at the point 0.5:

$$\theta_{X,Y} := 2 \cdot A_{X,Y}(0.5). \tag{5}$$

The extremal coefficient takes its minimal possible value of 1 if X and Y are comonotonic (so in particular it holds $\theta_{X,X} = 1$ for all X). The maximal possible value of 2

$$D_0(x,y) := \theta_{x,y} - 1$$

is obtained if X and Y are stochastically independent. To estimate the extremal coefficient, we use the madogram estimator as described in Ribatet et al. (2015) and Cooley et al. (2006) and rewrite $\theta_{X,Y}$ as

$$\theta_{X,Y} = \frac{1 + 2\nu_{X,Y}}{1 - 2\nu_{X,Y}} \tag{6}$$

with the madogram $\nu_{X,Y} = \tfrac{1}{2}\mathbb{E}[|F_X(X) - F_Y(Y)|]$. The madogram can be estimated by replacing F_X, F_Y with their empirical counterparts. For a data sample $(x_1, y_1), \ldots, (x_n, y_n)$, we then obtain

$$\hat{\nu}_{X,Y} = \frac{1}{2n(n+1)} \sum_{i=1}^{n} \left| \sum_{j=1}^{n} (\mathbf{1}_{x_j \le x_i} - \mathbf{1}_{y_j \le y_i}) \right|. \tag{7}$$

and consequently define an estimator

$$\hat{\theta}_{X,Y} = \frac{1 + 2\hat{\nu}_{X,Y}}{1 - 2\hat{\nu}_{X,Y}}. \tag{8}$$

Hierarchical clustering algorithms require a dissimilarity function $D : \mathcal{G} \times \mathcal{G} \to \mathbb{R}$ that must fulfil $D(g_1, g_2) = D(g_2, g_1) \geq 0$ and $D(g_1, g_1) = 0$ for all grid points $g_1, g_2 \in \mathcal{G}$ (for an introduction to hierarchical clustering algorithms see Murtagh and Contreras, 2012). Based on the properties of the extremal coefficient discussed above, we define such a dissimilarity function as

$$D_0(g_1, g_2) := \hat{\theta}_{X,Y} - 1 \tag{9}$$

with X and Y representing the GEV distributions at the grid points g_1 and g_2, respectively.

Note that the extremal coefficient is invariant under rank transformations and especially that it does not depend on the values of the GEV parameters of the marginal distributions (in fact, in Ribatet et al. (2015) and Cooley et al. (2006) it was only used in the special case of $\mathrm{GEV}(1,1,1)$ distributed margins, ~~but it can easily be extended to the general case~~). It may be desirable ~~also to include the similarity of the estimated GEV parameters in the dissimilarity measure used for the~~ to also include the dissimilarity of the marginal distributions in the clustering. As a further generalised dissimilarity measure we propose

$$D_\lambda(x_{g_1}, y_{g_2}) := (1 - \lambda) D_0(x_{g_1}, y_{g_2}) + \lambda \left(\frac{1}{3} d_\mu(x_{g_1}, y_{g_2}) + \frac{1}{3} d_\sigma(x_{g_1}, y_{g_2}) + \frac{1}{3} d_\gamma(x_{g_1}, y_{g_2}) \right), \tag{10}$$

~~with $d_p(x,y) = \frac{|p_x - p_y|}{\max_{a,b} |p_a - p_b|}$~~ where $\lambda \in [0,1)$ is a weighting parameter and with $d_\mu(g_1, g_2) := \frac{|\hat{\mu}_{g_1} - \hat{\mu}_{g_2}|}{\max_{h_1, h_2 \in \mathcal{G}} |\hat{\mu}_{h_1} - \hat{\mu}_{h_2}|} \in [0,1]$ the normalised distance between the location parameter estimates at the ~~points x and y, where p is one of the parameters μ, σ, γ and with $\lambda \in [0,1)$ a weighting parameter~~ grid points g_1 and g_2 (analogous for d_σ and d_γ). Instead of an equal weighting, it would also be possible to use different weights for d_μ, d_σ and d_γ, but the selection of a set of weights that is clearly better suited to describing GEV distribution dissimilarity is difficult. It could be argued to put more weight on the shape parameter since this parameter describes the heavy-tailedness of the distribution and therefore the strength of its extremes relative to the non-extreme values. On the other hand, we will see in the next section that the uncertainty in the shape parameter estimation is considerably higher than the uncertainty in the estimation of the other two parameters at least for our data, which would speak against weighting shape parameter differences too strongly.

~~Hierarchical clustering algorithms are well-known, for an introduction see Murtagh and Contreras (2012). To choose an optimal~~ To choose a suitable number of clusters, we consider an approach by Salvador and Chan (2004) called the L-Method. In each step of the hierarchical clustering, the two clusters with minimal dissimilarity are combined, therefore we can plot the number of clusters versus the dissimilarity between them, resulting in a graph called the evaluation graph. The dissimilarity between clusters necessarily grows as the total number of clusters is reduced. The idea of Salvador and Chan (2004) is to find a point from which on the growth rate of the dissimilarity measure increases considerably. It can then be expected that the clusters up to this point combine rather similar data points, while combining them to larger ones would yield artificial results. To determine such a point of change, in the first step, a suitable range of the number of clusters is selected. For our example, we ~~use~~ consider different ranges starting with 10 and having no more than 550 clusters. Now, for each possible point of change c in this range, the ~~x-axis~~ horizontal axis of the graph is divided into the two parts to the left and the right of ~~the change~~ that point, and a linear regression line is fitted to each of the two partial graphs. The root mean squared errors (~~RMSE's~~RMSEs) of the

250 two regression lines are weighted with the number of points involved in the regression analysis and summed up. The ~~change point~~ point of change with the minimal combined RMSE is chosen as the ~~optimal~~ suitable cluster number. As an alternative method, we set the number of clusters to the highest possible number such that a fixed threshold dissimilarity between clusters is not exceeded (Threshold method). This number can easily be read off ~~on~~ of the evaluation graph.

4   Results

255 We start with calculating for each ~~annually maximised data point its~~ grid point the empirical mean and standard deviation of the annually maximised data, as can be seen in Fig. 1. In most regions, similar mean values can be observed. A notable overestimation of the annual maxima of monthly precipitation by the climate model takes place in the Himalayas and along the western continent coasts of the Americas. Underestimation occurs most prominently in the Amazon region and parts of Central America, as well as in Bangladesh and East Asia. Looking at the standard deviation, a similar pattern as for the empirical mean

260 can be observed, but with a stronger tendency for underestimation, which occurs also in India and the northern part of Australia. In Fig. 2 a) and b), quantile-quantile plots (QQ-plots) of empirical mean and standard deviation ~~can be seen~~are displayed. The quantiles of the empirical mean are in general similar, but the highest quantiles show a strong discrepancy. Regarding the standard deviation, this tendency is much more pronounced, corresponding to the larger areas of underestimation of empirical standard deviation we ~~saw in 1. In Fig. 2 c), the~~ identified in Fig. 1. The difference in empirical mean and the difference in

265 empirical standard deviation are plotted against each other ~~, and it is clearly visible that~~ in Fig. 2 c). It is visible that in many cases, overestimation (underestimation) of the empirical mean corresponds also to overestimation (underestimation) of the empirical standard deviation. A similar case of heteroscedasticity has also been noted in Lohmann (2018) when investigating Holocene climate.

270 As pointed out by Katz and Brown (1992), the frequency of extreme events is strongly influenced by changes (or, in this case, ~~overestimation~~misestimation) of the mean as well as of the variance of a distribution. Therefore, ~~a systematic~~ an over- and underestimation of extremes can be expected in certain regions based on the results in Figs. 1 and 2.

Fitting the GEV distributions to the data and applying KS-Tests to check the goodness of fit, the hypothesis of a GEV distribution with the estimated parameters is not rejected for nearly all grid points in both observational and climate model data,

275 except for parts of the Sahara and some isolated points.

The three GEV parameters estimated are location, scale and shape, with location and scale very roughly corresponding to mean and variance, and the shape parameter yielding information about the degree of heavy-tailedness. The estimated parameter values are shown in Fig. 4. In Fig. 5, the differences between model and ~~observations~~ observational parameters

280 are shown. Shaded areas are areas in which the model parameter falls into the 95% confidence interval of the corresponding observation parameter and vice versa. We can observe a ~~strong~~ similarity between the anomaly of the location parameters and the anomaly of the empirical means discussed above, and likewise a similarity between the anomalies of scale parameters and
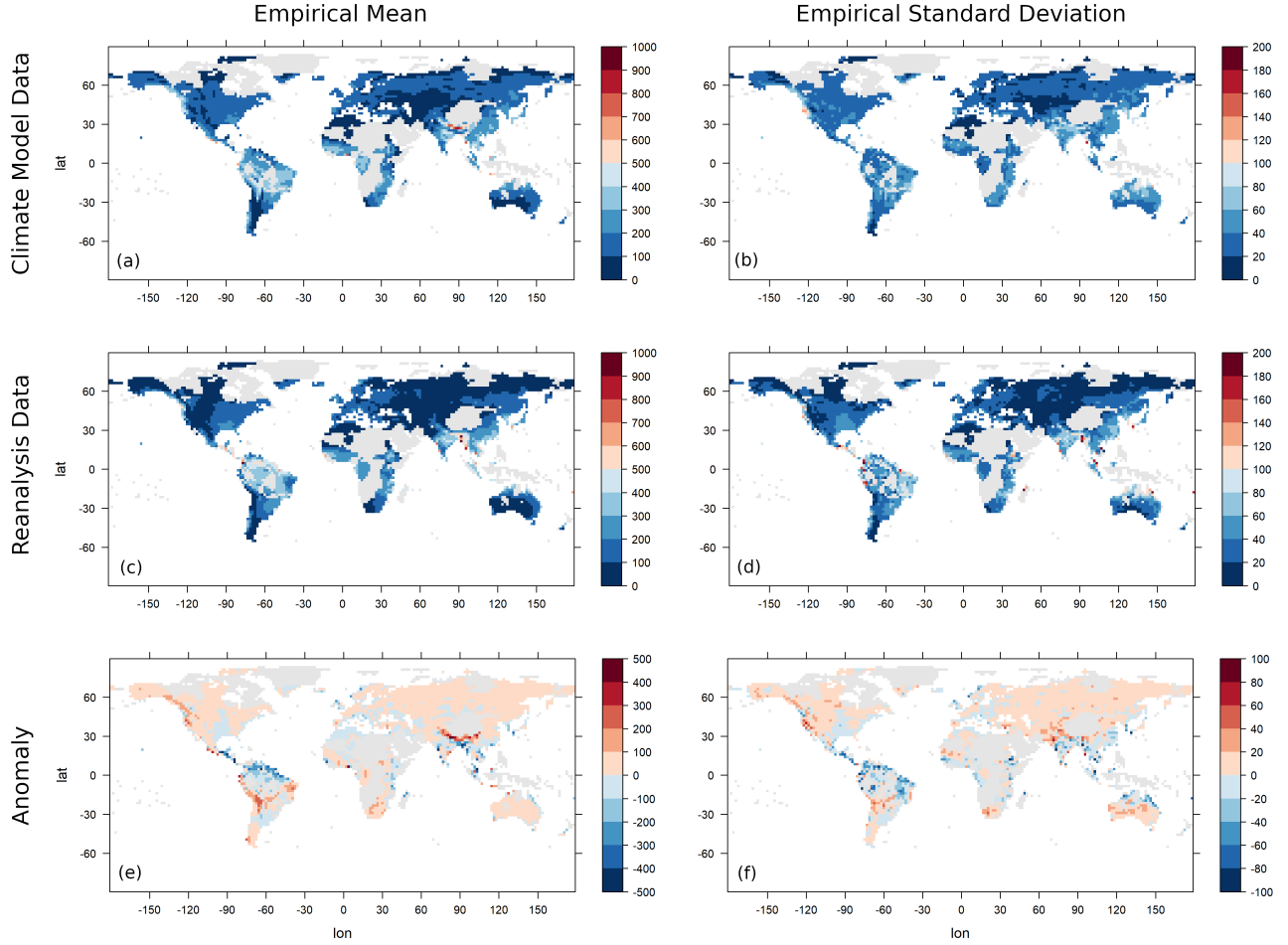
Figure 1. The empirical mean (a, c, e) and empirical standard deviation (b, d, f) of the annual maxima of monthly precipitation of the ~~CRU TS4.04 reanalysis~~ AWI-ESM model data set (a, b) and of the ~~AWI-ESM model~~ CRU TS4.04 reanalysis data set (c, d) and their difference (~~reanalysis minus~~ model data minus reanalysis data; e, f). Values exceeding the scale limits are truncated. Units are mm/month.
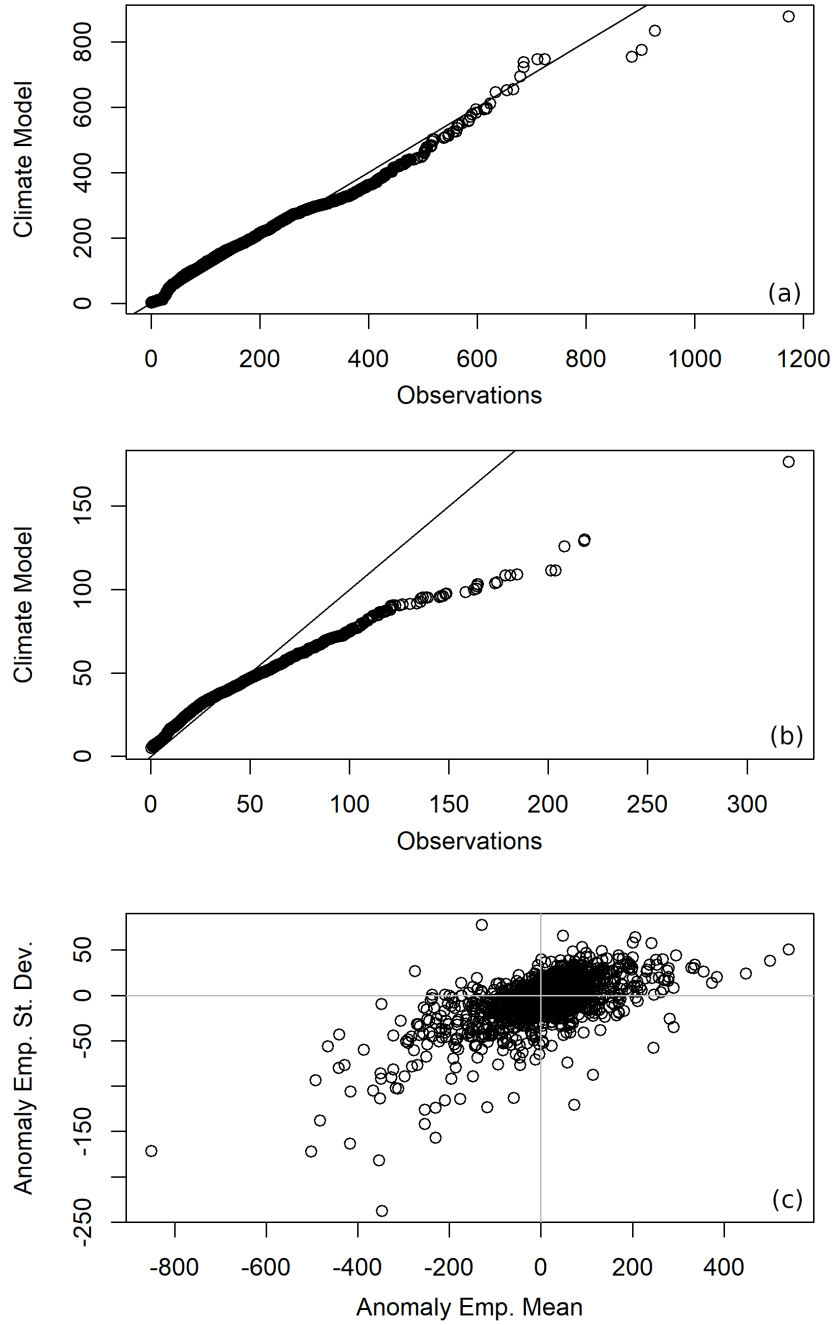
Figure 2. QQ-Plots comparing the empirical mean values (a) and the empirical standard deviations (b) ~~and~~ of the annually maximised monthly precipitation of the CRU TS4.04 reanalysis data set and of the AWI-ESM model data set. Deviance of empirical mean and standard deviation plotted against each other (c). Units are $\mathrm{mm/month}$.
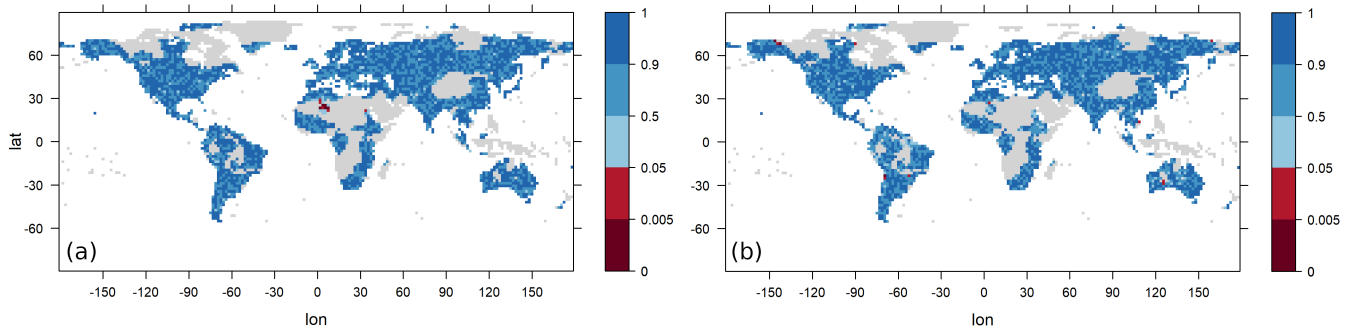
Figure 3. P-values of Kolmogorov-Smirnov tests for the hypothesis that the data follow a GEV distribution with parameters estimated using probability-weighted moments. Test results for the AWI-ESM climate model (a) and for the CRU TS4.04 reanalysis data (b).

empirical standard deviations. For the location parameter, we ~~often~~ observe high differences quite often, and the parameters estimated for one data set seldom fall into the confidence interval derived from the other data set. The ~~confidence intervals of the~~ estimated scale parameters are ~~met more often~~ covered more often by the confidence intervals derived from the other data set, although there are also large regions with a high difference in the two estimates. The estimated shape parameters ~~often lie within~~ are covered by the confidence intervals at many locations, but it needs to be noted that the estimator of the shape parameter is known to be sensitive to small variations in the data. Therefore, the confidence intervals calculated using the parametric bootstrap tend to be large and not particularly informative. In Fig. 6, the anomalies of the 95% upper quantiles of the estimated GEV distributions are depicted, again with ~~shading indicating areas lying in~~ shaded areas indicating quantiles lying within the confidence levels determined using parametric bootstrap. Climate extremes are most strongly overestimated by the model in the ~~mountanious~~ mountainous regions of the Himalaya, the Andes and the Rocky Mountains. An underestimation of climate extremes takes place most notably in the Amazon region and parts of eastern Asia. This corresponds well to the regions of over- and underestimation of the empirical means and standard deviations and the implications of such misestimations discussed above.

We apply the hierarchical clustering algorithms using the two dissimilarity measures D_0 and $D_{0.25}$ as introduced in the previous section. The numbers of clusters determined using the L-Method with selected cluster ranges (from 10 to a maximal number of clusters m) and using the threshold method with selected threshold dissimilarities h is documented in Table 1.

The results of the L-Method ~~strongly depend on the~~ seem to depend rather strongly on the data set investigated and the value of m ~~and show a fairly inconsistent behaviour~~(compare for example the results for $m = 250$ and $m = 300$ for measure D_0), making this method ~~not very~~ less suitable for the comparison of two data sets. The threshold method ~~consistently~~ generally predicts a similar, but in most cases slightly lower cluster number for observational data than for climate model data. In Fig. 7, the clusters for both data sets are depicted using the threshold method for dissimilarity measure D_0 with threshold $h = 0.825$ as well as for dissimilarity measure $D_{0.25}$ with threshold $h = 0.65$.
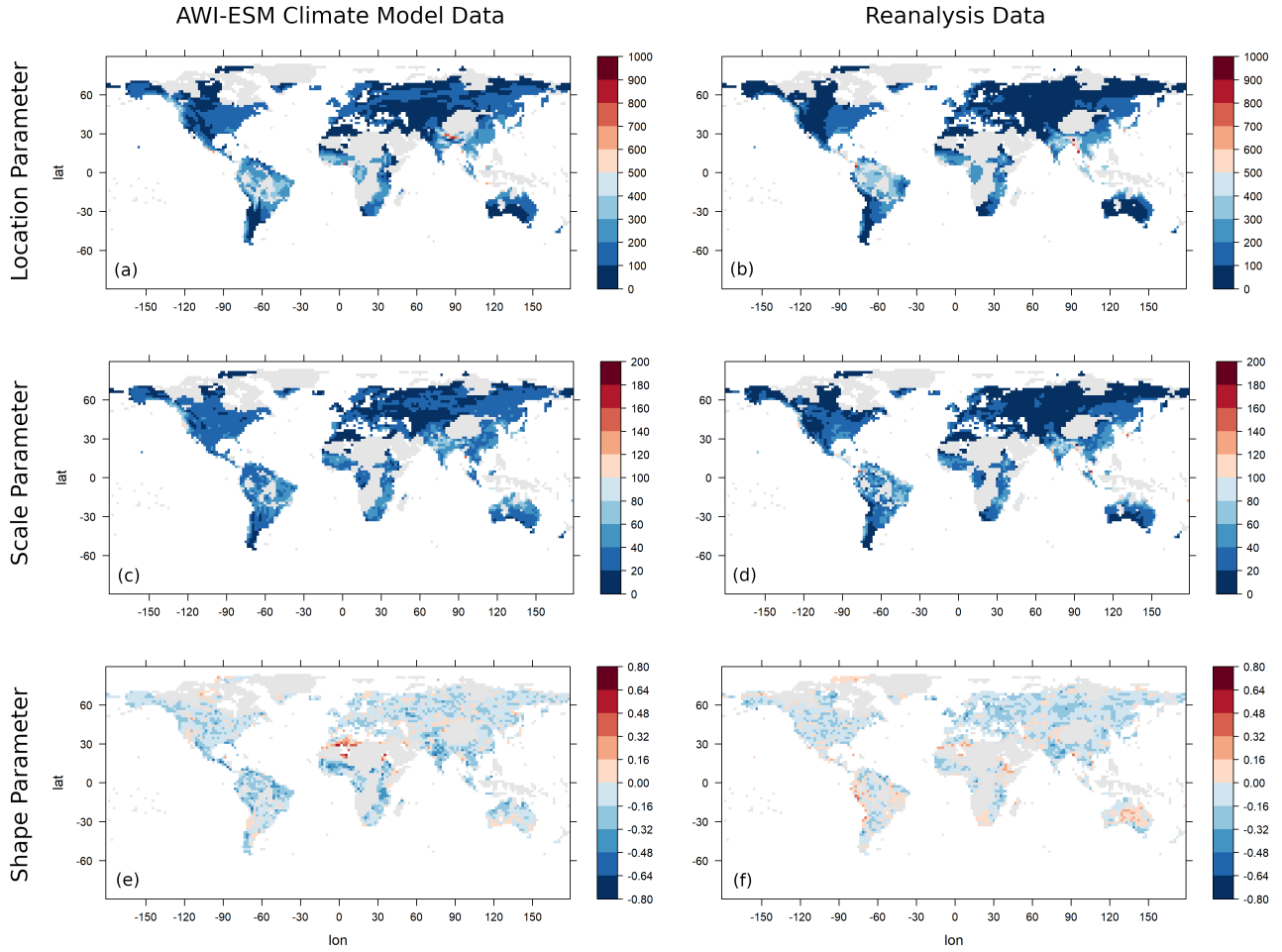
Figure 4. The estimated GEV parameters location (a, b), scale (c, d) and shape (e, f) for AWI-ESM climate model data (a, c, e) and for reanalysis data (b, d, f). Values exceeding the scale limits are truncated. Units are $\mathrm{mm/month}$.
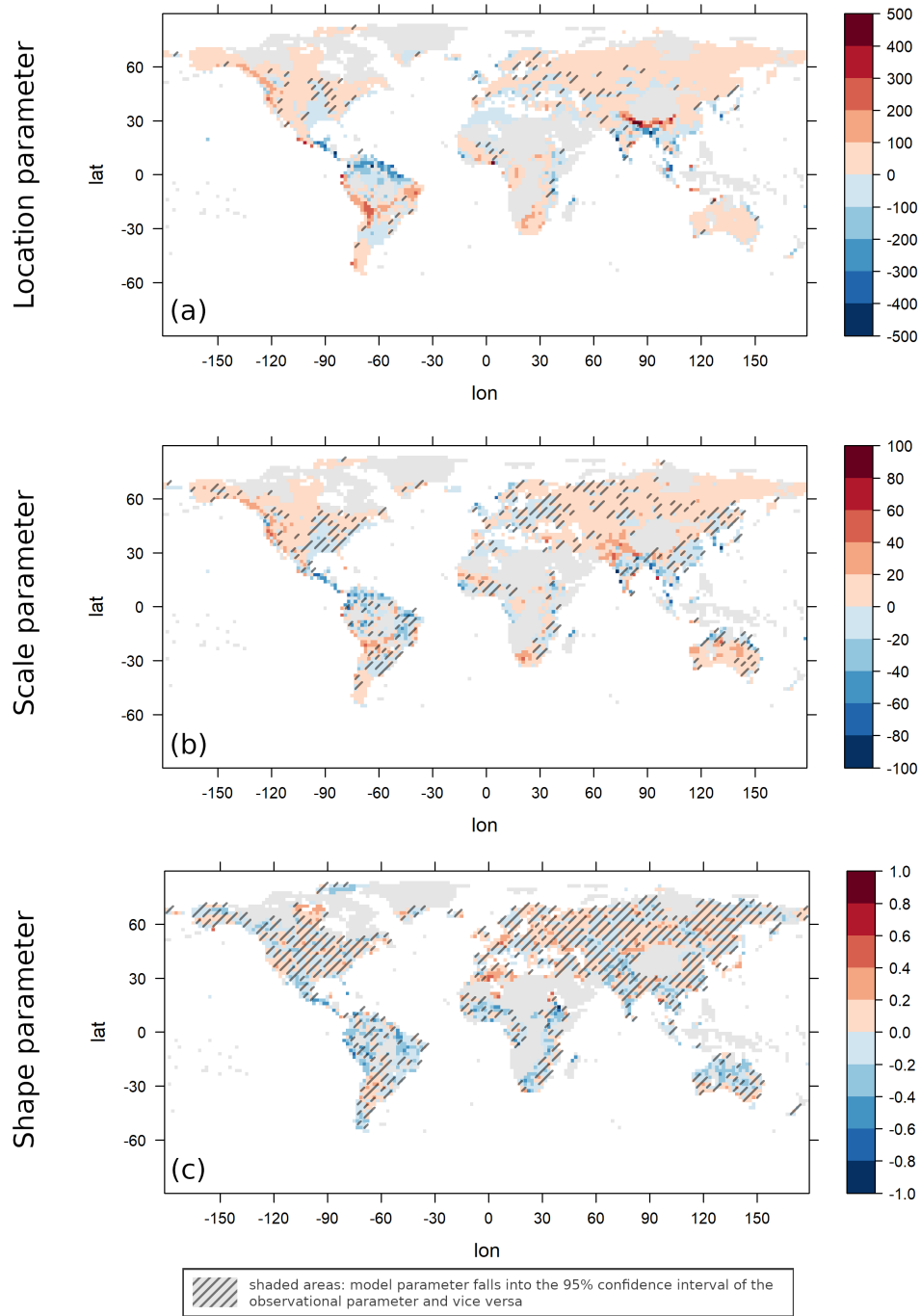
Figure 5. Difference between AWI-ESM model and observational GEV parameter estimates: Location parameter (a), scale parameter (b) and shape parameter (c). Values exceeding the scale limits are truncated. Units are $\mathrm{mm/month}$.

shaded areas: model quantile falls into the 95% confidence interval of the observational quantile and vice versa
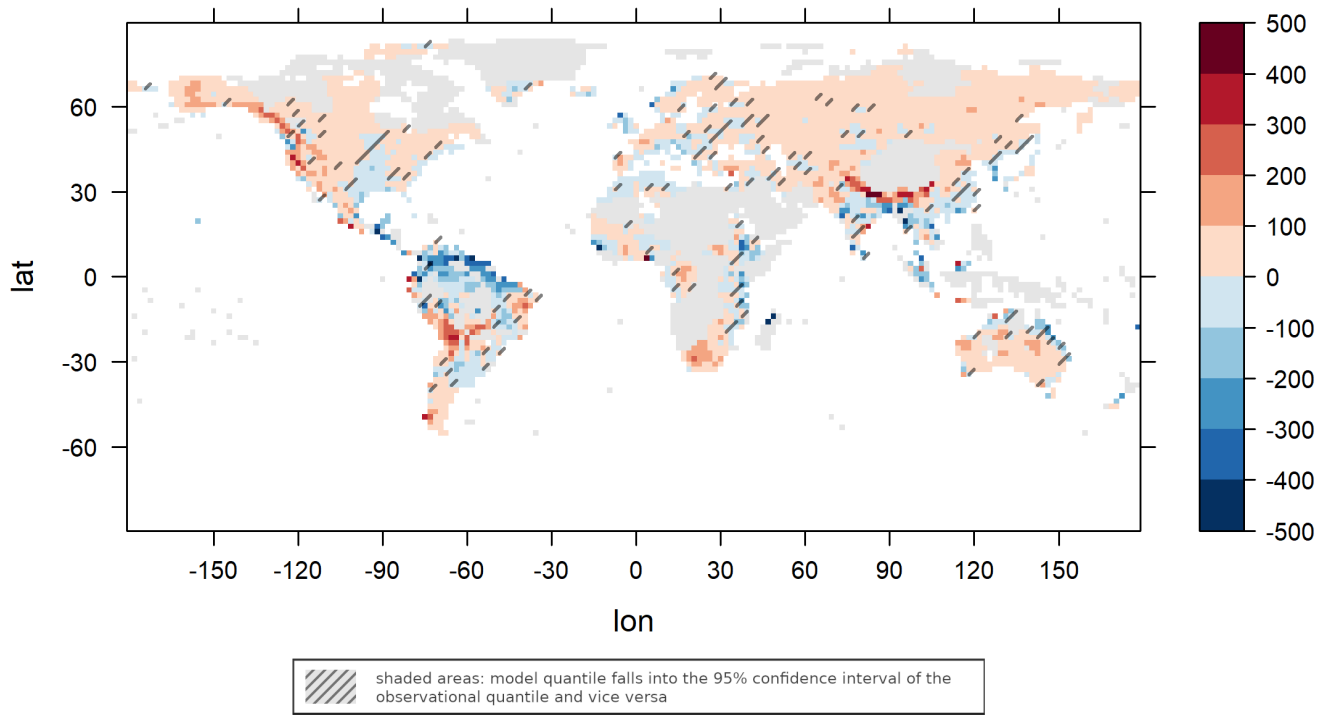
Figure 6. Difference of the 0.95-quantiles of the estimated GEV distribution for AWI-ESM model and observational data. Values exceeding the scale limits are truncated. Units are $\mathrm{mm/month}$.

Table 1. The number of clusters for AWI-ESM climate model and observational data determined with the L-Method (above the middle line) and the threshold method (below the middle line) for different ranges/thresholds and for dissimilarity measure D_0 (left) and $D_{0.25}$ (right).

$\mathbf{D_0}$	Model AWI-ESM	Obs. Observations		$\mathbf{D_{0.25}}$	Model AWI-ESM	Obs. Observations
$m = 250$	64	146		$m = 250$	187	102
$m = 300$	148	148		$m = 300$	165	142
$m = 400$	200	296		$m = 400$	223	140
$m = 500$	234	291		$m = 500$	232	265
$h = 0.85$	143	127		$h = 0.675$	118	109
$h = 0.825$	188	177		$h = 0.65$	165	167
$h = 0.8$	232	221		$h = 0.625$	219	220
$h = 0.775$	280	254		$h = 0.6$	281	265

To exemplify the differences and similarities in the clusterings, we have a closer look at Europe in the D_0-clusterings. In
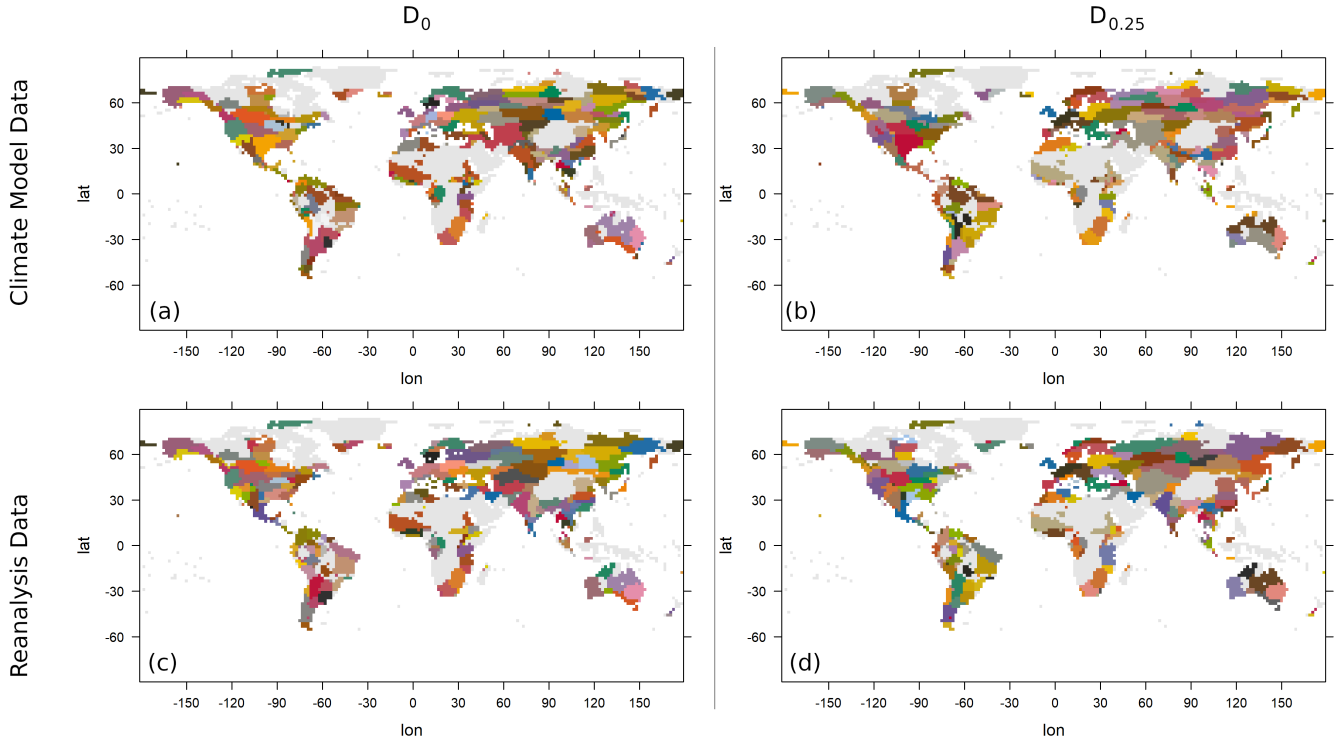
Figure 7. Clustering of AWI-ESM model data (a, b) and observational data (c, d) with the dissimilarity measure D_0 and threshold $h = 0.825$ (a, c) and with dissimilarity measure $D_{0.25}$ and threshold $h = 0.65$ (b, d).

the model data, there is one cluster covering western Spain and Portugal, one cluster covering eastern Spain, and one cluster consisting of southern France and Italy. Great Britain and Denmark are in the same cluster, the northern parts of France together with Belgium and the Netherlands in another one. One cluster covers Germany and Switzerland, and in Eastern Europe we see several clusters covering larger areas in the longitudinal direction, for example one cluster over Poland, one over Ukraine, and one over Turkey and Greece. The clusters in the observational dataset show a slightly different picture: Here, the whole Iberian Peninsula is in one cluster, and one large cluster extends over northern France, Belgium, the Netherlands and Germany to the western parts of Poland. On the other hand, Great Britain and Denmark are now in two separate clusters. Regarding other parts of the world, it is worth noting that in all four clusterings a large cluster cluster covering the Sahara (or at least all parts of it for which there are observations available) can be identified. There are no clusters extending over two regions that are very far apart from each other, and in general clusters tend to cover more area in the longitudinal direction than in the latitudinal one.

320 For the AWI-ESM, we calculated an AWQD of 52.98, making it the third-best of all 27 CMIP6 models analysed. A full table of the models and their AWQDs is provided in the supplement to this paper. In Fig. 8, the AWQDs are plotted against the model resolution (the total number of model grid points in units of 10^4). A linear regression (red line; intercept: 73.310, slope: -2.368) indicates that models with a higher resolution have a tendency to describe extremal precipitation better. A test on the significance of the slope parameter (null hypothesis of the slope parameter being equal to zero) was significant at the

325 5% level with a p-value of 0.0357. The best model in terms of the AWQD is the high-resolution model EC-Earth3-Veg-LR (EC-Earth Consortium, 2020) with a value of 44.71. We will now discuss results for this model in more detail, while results for the other models can be found in the supplement. For the EC-Earth3-Veg-LR, the estimated GEV parameters and anomalies are shown in Fig. 9. The differences of the 95% quantiles are depicted in Fig. 10. The numbers of clusters determined using the L-Method and the threshold method are found in Table 2 and images of clusterings are shown in Fig. 11. QQ-Plots and

330 plots of KS-Tests are similar to the corresponding plots for the AWI-ESM and can be found in the supplement to this paper. The EC-Earth3-Veg-LR model predicts climate extremes better than the AWI-ESM in the Himalayas and in the Amazon region (compare Fig. 6 to Fig. 10), while it overestimates precipitation extremes more strongly than the AWI-ESM at the western coast of South America. The number of clusters is in general higher than for the AWI-ESM, in part probably due to the higher model resolution (320×160 compared to 192×96). Note that this increased resolution is also the reason for the different values for

335 the cluster numbers of the reanalysis data in Tables 1 and 2, because reanalysis data were in each case interpolated to the climate model resolution. When comparing again the clusters over Europe using the D_0 dissimilarity measure, it can be observed that in the western part of Europe, model and observational clusters are in general similar, with only slight differences over the Iberian Peninsula and with an area covering southern France and northern Italy that is in one cluster in the model data and in two different clusters in the observational data. In Eastern Europe and Scandinavia, the differences between the clusterings are

340 larger and it is more difficult to see correspondences. The general remarks that have been made about the clusterings while discussing the AWI-ESM data also apply here.
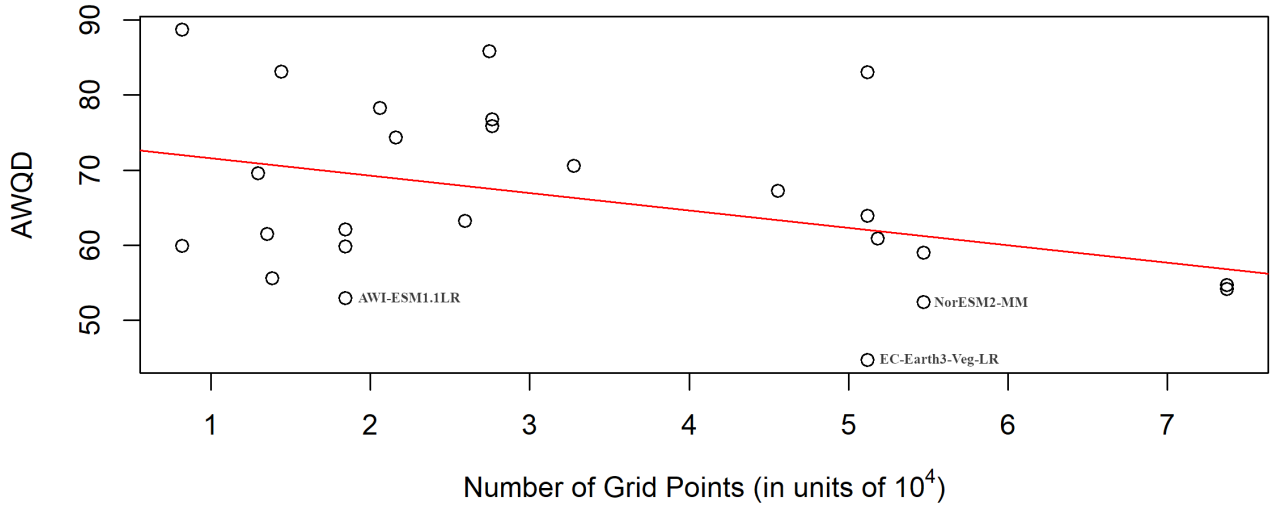
Figure 8. The Average Weighted Quantile Difference (AWQD) of the 27 CMIP6 models considered plotted against the model resolution (number of model grid points in units of 10^4). In red: Linear regression line (intercept 73.310, slope -2.368).

Table 2. The number of clusters for EC-Earth3-Veg-LR climate model and observational data determined with the L-Method (above the middle line) and the threshold method (below the middle line) for different ranges/thresholds and for dissimilarity measure D_0 (left) and $D_{0.25}$ (right).

D_0	EC-Earth3-Veg-LR	Observations	$D_{0.25}$	EC-Earth3-Veg-LR	Observations
$m = 250$	76	89	$m = 250$	113	67
$m = 300$	141	90	$m = 300$	117	67
$m = 400$	181	94	$m = 400$	129	154
$m = 500$	184	272	$m = 500$	146	282
$h = 0.85$	173	145	$h = 0.675$	131	116
$h = 0.825$	224	186	$h = 0.65$	203	166
$h = 0.8$	299	240	$h = 0.625$	276	225
$h = 0.775$	366	272	$h = 0.6$	358	279

5 Conclusions

We presented approaches and methods to validate climate model outputs by comparing their extremal behaviour to the extremal behaviour of observational data. To illustrate these methods, we compared precipitation extremes between the ~~AWI Earth System Model~~ AWI-ESM and the CRU TS4.04 data set of reanalysed observations. After an analysis of empirical ~~statistics~~statistical parameters, we fitted the data to GEV distributions and ~~analyse~~analysed the differences in estimated pa-
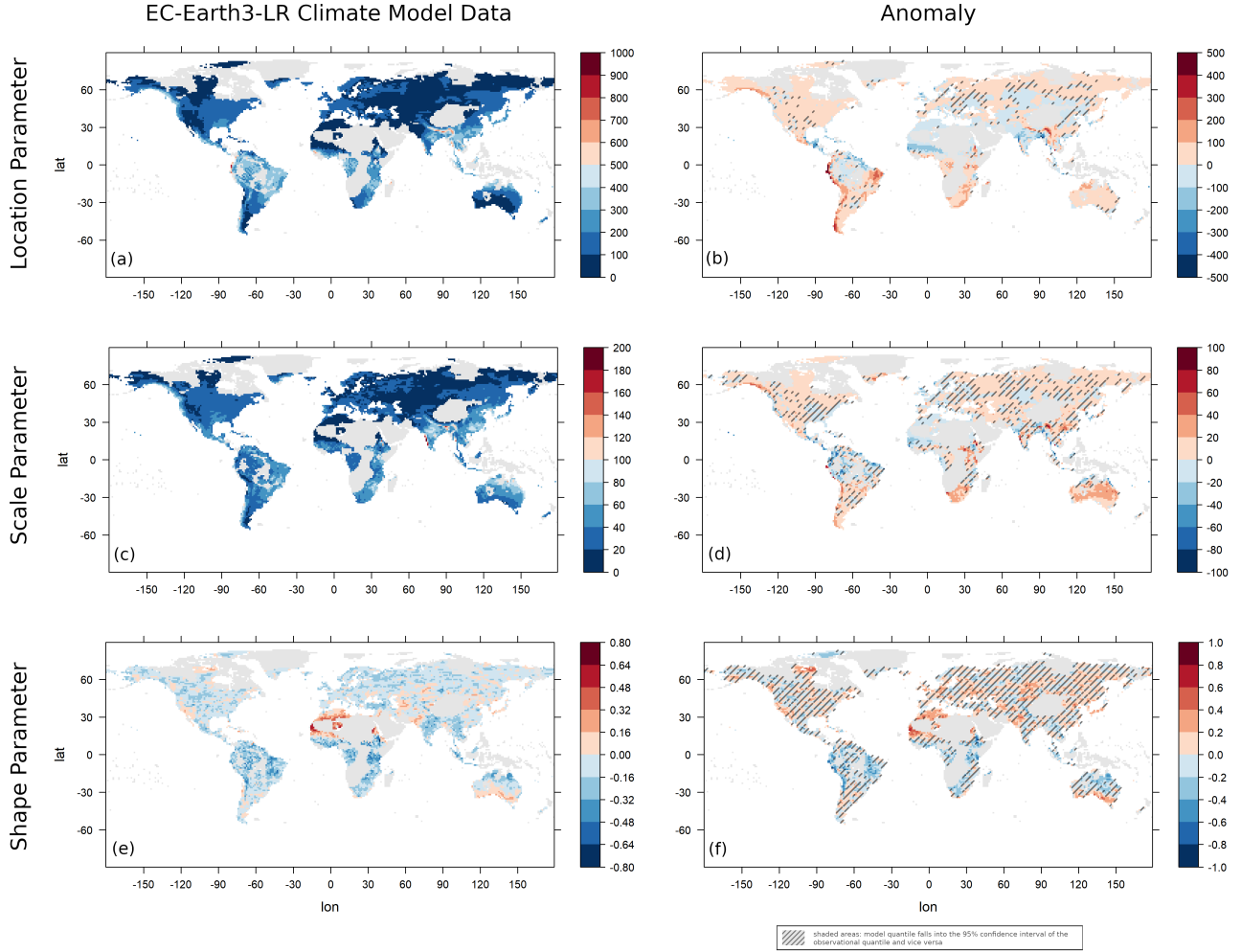
Figure 9. EC-Earth3-Veg-LR climate model estimated GEV parameters (a, c, e) and their anomaly compared to the reanalysis GEV parameters (b, d, f). The GEV parameters are location (a, b), scale (c, d) and shape (e, f). Values exceeding the scale limits are truncated. Units are mm/month.
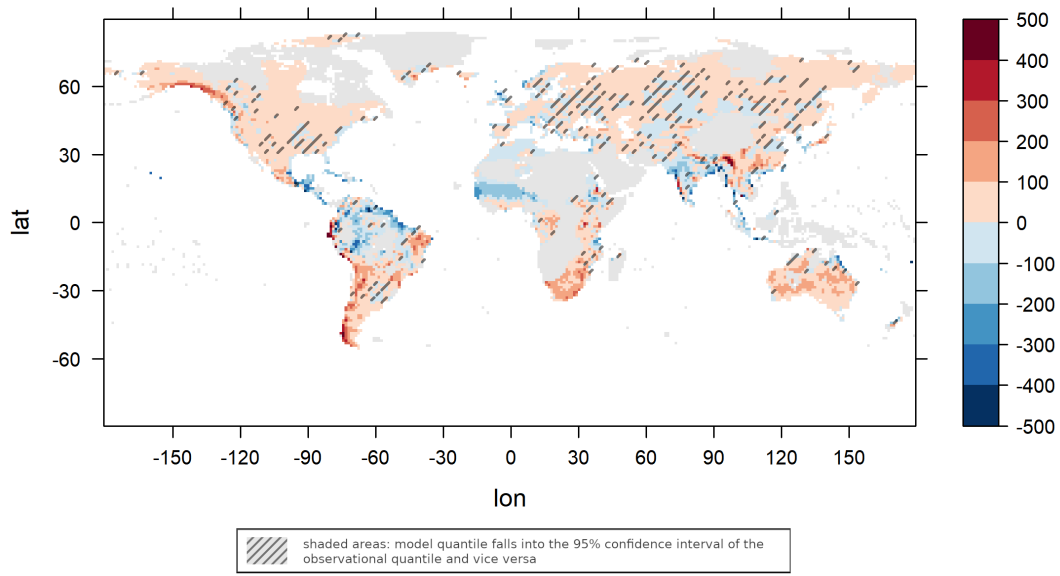
Figure 10. Difference of the 0.95-quantiles of the estimated GEV distribution for EC-Earth3-Veg-LR model and observational data. Values exceeding the scale limits are truncated. Units are mm/month.
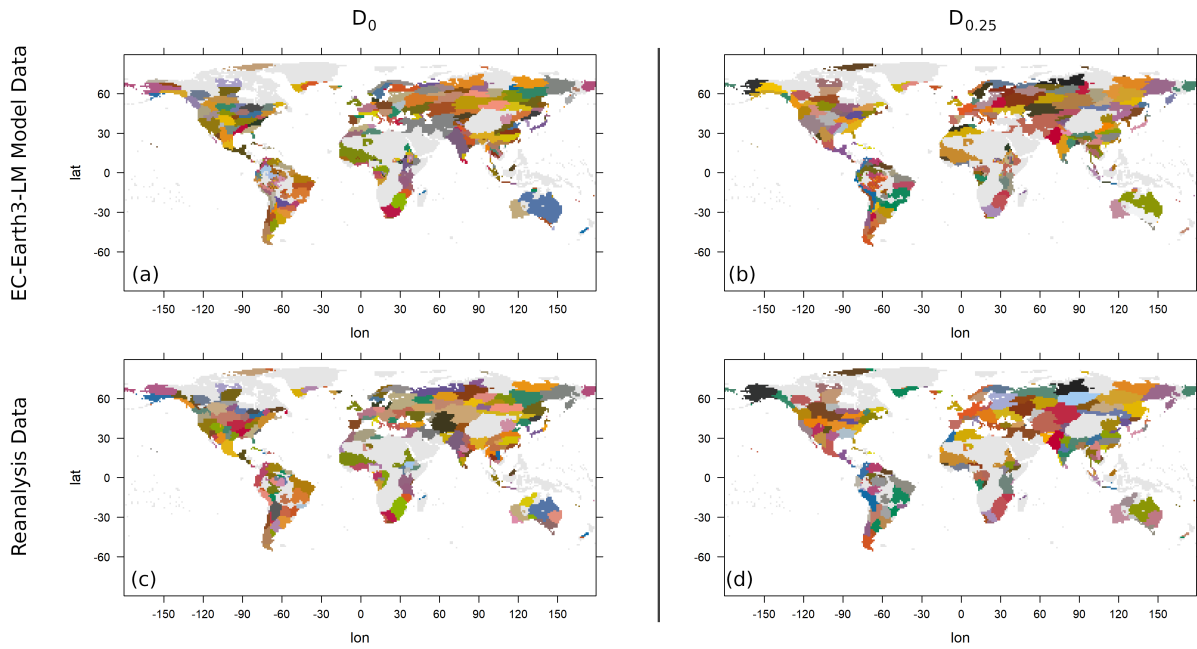
Figure 11. Clustering of EC-Earth3-Veg-LR model data (a, b) and observational data (c, d) with the dissimilarity measure D_0 and threshold $h = 0.825$ (a, c) and with dissimilarity measure $D_{0.25}$ and threshold $h = 0.65$ (b, d).

rameters. Then we continued with an analysis of spatial concurrence of extremes based on a hierarchical clustering approach

and a dissimilarity measure derived from bivariate copula theory. While the empirical statistics are similar for many parts of

350 the world, we can also identify larger regions of ~~a continuous~~ over- and underestimation of empirical means and standard

deviations by the climate model. These misestimations often go hand in hand with a similar misestimation of the standard

deviation (heteroscedasticity), although for the standard deviation a stronger tendency for underestimation can be observed.

Misestimations of mean and standard deviations translate into a misestimation of extreme values, and this can be confirmed

by the comparison of the fitted GEV distribution parameters and the 0.95-quantiles derived from them. The shape parameter,

355 indicative of the heavy-tailedness of the distribution, is in general similar between model and observational data, but because

of the difficulties in reliably estimating this parameter from data (that are in turn a result of the rareness of extreme events in

the data) these results have to be taken with caution.

The cluster analysis based on spatial dependencies and the ~~occurence~~ occurrence of concurrent extremes shows that there is

360 generally a good agreement between identified clusters. Also the number of clusters is in general similar, with a slight tendency

for a higher cluster number in the model data. Since it is mostly large-scale weather events and teleconnections contributing to

concurrent climate extremes, this ~~indicates~~ may indicate that the basic physical behaviour underlying them is in general well

captured by the ~~AWI Earth System Model. Further analysis~~ AWI-ESM. Further analyses can be conducted to investigate in

detail the reasons for different clusterings over selected regions.

365

In addition to the AWI-ESM, several other CMIP6 models are also analysed. A comparison of the model accuracy, measured

using an averaged quantile difference, shows a tendency for higher-dimensional models to capture extremal behaviour better.

In this work, ~~we use~~ a clustering algorithm based on bivariate ~~copulae~~ extremal coefficients is used to perform a spatial

370 analysis of extreme values. ~~Another possible approach is the direct application of multivariate copulae. While parametric~~

~~copulae families are applicable only to a very limited extent in high dimensions, the use of a non-parametric estimator based~~

~~on Bernstein polynomials is a promising idea. This technique enabled Marcon et al. (2014) to estimate the common distribution~~

~~of up to seven variables in their analysis of French precipitation data. Copulae based on Bernstein polynomials are also used~~

~~in multivariate extreme value analysis with a focus on multiple testing (Neumann et al., 2019). In global climate models, the~~

375 ~~number of dimensions is much higher than seven and the approach by Marcon et al. (2014) is not directly transferable. Based~~

~~on another approach, the multivariate spatial distribution of precipitation has also been described~~ Extremal coefficients are

also used to model multivariate spatial distributions of extremal precipitation using max-stable processes~~, first~~. This method

was first developed by Smith (1990) and Schlather (2002) and then extended by Opitz (2013) and Ribatet et al. (2015)~~. This~~

~~procedure~~, and it is successfully used to model precipitation over Switzerland (Ribatet, 2017). The models based on max-

380 stable processes assume spatial ~~stationary~~ stationarity (i.e. the spatial dependence between two points depends only on their

distance). This assumption is justifiable for small regions like Switzerland, but it makes the models in their present form

~~unsuitable~~ not well suitable for global data. Castro-Camilo and Huser (2020) created a model for the spatial distributions of

extreme tail dependencies based on factor copulae, allowing them to use the relaxed assumption of local spatial stationarity and therefore to apply their model to the whole contiguous United States. From the area of parametric copulae, also vine

385 copulae have been employed to model precipitation data by Vernieuwe et al. (2015) and by Nazeri Tahroudi et al. (2021). A further possibility is the application of non-parametric multivariate copulae. Marcon et al. (2014) used an estimator based on Bernstein polynomials to model the common distribution of up to seven variables in their analysis of French precipitation data. Copulae based on Bernstein polynomials are also used in multivariate extreme value analysis with a focus on multiple testing (Neumann et al., 2019). In global climate models, the number of dimensions is much higher than seven and the method by

390 Marcon et al. (2014) is not directly transferable.

The clustering approach presented here focuses on the comparison of extremal events at different locations, thereby supplementing the analyses of climate extremes that are often focused on extremes at a specific location (Zhang et al., 2011). An application to daily data that has been annually or seasonally maximised , is also possible, but beyond the scope of this pa-

395 per. Besides, the method can be used for the comparison of ensembles of models (see Sillmann et al., 2013; Kim et al., 2020) In order to investigate extreme precipitation within the area covered by one cluster in more detail, the spatially stationary max-stable models or the copulae-based models mentioned above could be employed. Most of the clusters cover only a small region, therefore spatial stationarity might be a reasonable assumption, although it is not a direct consequence of the data being in the same cluster. In addition to model validation, the definition of regions with concurrent extremes may turn out useful

400 for assessments of risks in a an economical context and for insurance. It needs to be noted, though, that extremes in climate models and in gridded reanalysis data sets tend to be damped because of the spatial averaging performed during the creation of the data (Bador et al., 2020b). Another possible field of application is palaeoclimatology. Spatial The spatial distribution of precipitation extremes is known to have changed markedly in the past (Lohmann et al., 2020; Ionita et al., 2021b), and clustering based on climate models could be used to generalise the sparse existing palaeoclimatic data to larger regions.

405 *Code and data availability.* The CRU TS4.04 reanalysis data are available at https://catalogue.ceda.ac.uk/uuid/89e1e34ec3554dc98594a5732622bce9. The AWI-ESM climate model data are available under https://www.doi.org/10.22033/ESGF/CMIP6.9328 and the EC-Earth3-Veg-LR model data can be found under https://doi.org/10.22033/ESGF/CMIP6.4702. The software code (in R) used for the analyses is provided in the supplementary material to this paper.

Author contributions. Initial concept by TD and GL. JC led the writing of the paper and implemented the statistical data diagnostics. TD

410 contributed to statistical methodology. GL contributed to the climatological analysis. All authors read and approved the manuscript.

Competing interests. The authors declare that they have no conflict of interest.

Acknowledgements. The authors are grateful to Manfred Mudelsee for constructive discussions and helpful suggestions. The authors also would like to thank GMD editor Julia Hargreaves and the editorial team as well as the reviewers Anna Kiriliouk and Qingxiang Li for their useful and constructive feedback. We acknowledge the World Climate Research Programme, which, through its Working Group on Coupled

415   Modelling, coordinated and promoted CMIP6. We thank the climate modelling groups for producing and making available their model output, the Earth System Grid Federation (ESGF) for archiving the data and providing access, and the multiple funding agencies that support CMIP6 and ESGF. JC is funded through the Helmholtz School for Marine Data Science (MarDATA), Grant No. HIDSS-0005. GL receives funding through "Ocean and Cryosphere under climate change" in the Program "Changing Earth - Sustaining our Future" of the Helmholtz Society and PalMod through BMBF.

References

Acero, F. J., García, J. A., and Gallego, M. C.: Peaks-over-Threshold Study of Trends in Extreme Rainfall over the Iberian Peninsula, J Climate, 24, 1089 – 1105, https://doi.org/10.1175/2010JCLI3627.1, 2011.

Ackermann, L., Danek, C., Gierz, P., and Lohmann, G.: AMOC Recovery in a Multicentennial Scenario Using a Coupled Atmosphere-Ocean-Ice Sheet Model, Geophys Res Lett, 47, https://doi.org/https://doi.org/10.1029/2019GL086810, 2020.

Bador, M., Boé, J., Terray, L., Alexander, L. V., Baker, A., Bellucci, A., Haarsma, R., Koenigk, T., Moine, M.-P., Lohmann, K., Putrasahan, D. A., Roberts, C., Roberts, M., Scoccimarro, E., Schiemann, R., Seddon, J., Senan, R., Valcke, S., and Vanniere, B.: Impact of Higher Spatial Atmospheric Resolution on Precipitation Extremes Over Land in Global Climate Models, J Geophys Res-Atmos, 125, e2019JD032 184, https://doi.org/https://doi.org/10.1029/2019JD032184, 2020a.

Bador, M., Boé, J., Terray, L., Alexander, L. V., Baker, A., Bellucci, A., Haarsma, R., Koenigk, T., Moine, M.-P., Lohmann, K., Putrasahan, D. A., Roberts, C., Roberts, M., Scoccimarro, E., Schiemann, R., Seddon, J., Senan, R., Valcke, S., and Vanniere, B.: Impact of Higher Spatial Atmospheric Resolution on Precipitation Extremes Over Land in Global Climate Models, Journal of Geophysical Research: Atmospheres, 125, e2019JD032 184, https://doi.org/https://doi.org/10.1029/2019JD032184, 2020b.

Bargaoui, Z. and Bárdossy, A.: Modeling short duration extreme precipitation patterns using copula and generalized maximum pseudo-likelihood estimation with censoring, Adv Water Resour, 84, 1–13, https://doi.org/https://doi.org/10.1016/j.advwatres.2015.07.006, 2015.

Bernard, E., Naveau, P., Vrac, M., and Mestre, O.: Clustering of Maxima: Spatial Dependencies among Heavy Rainfall in France, J Climate, 26, 7929 – 7937, https://doi.org/10.1175/JCLI-D-12-00836.1, 2013.

Brierley, C. M., Zhao, A., Harrison, S. P., Braconnot, P., Williams, C. J. R., Thornalley, D. J. R., Shi, X., Peterschmitt, J.-Y., Ohgaito, R., Kaufman, D. S., Kageyama, M., Hargreaves, J. C., Erb, M. P., Emile-Geay, J., D'Agostino, R., Chandan, D., Carré, M., Bartlein, P. J., Zheng, W., Zhang, Z., Zhang, Q., Yang, H., Volodin, E. M., Tomas, R. A., Routson, C., Peltier, W. R., Otto-Bliesner, B., Morozova, P. A., McKay, N. P., Lohmann, G., Legrande, A. N., Guo, C., Cao, J., Brady, E., Annan, J. D., and Abe-Ouchi, A.: Large-scale features and evaluation of the PMIP4-CMIP6 *midHolocene* simulations, Clim Past, 16, 1847–1872, https://doi.org/10.5194/cp-16-1847-2020, 2020.

Brown, J. R., Brierley, C. M., An, S.-I., Guarino, M.-V., Stevenson, S., Williams, C. J. R., Zhang, Q., Zhao, A., Abe-Ouchi, A., Braconnot, P., Brady, E. C., Chandan, D., D'Agostino, R., Guo, C., LeGrande, A. N., Lohmann, G., Morozova, P. A., Ohgaito, R., O'ishi, R., Otto-Bliesner, B. L., Peltier, W. R., Shi, X., Sime, L., Volodin, E. M., Zhang, Z., and Zheng, W.: Comparison of past and future simulations of ENSO in CMIP5/PMIP3 and CMIP6/PMIP4 models, Clim Past, 16, 1777–1805, https://doi.org/10.5194/cp-16-1777-2020, 2020.

Carvalho, M., Melo-Gonçalves, P., Teixeira, J., and Rocha, A.: Regionalization of Europe based on a K-Means Cluster Analysis of the climate change of temperatures and precipitation, Phys Chem Earth Pt A/B/C, 94, 22–28, https://doi.org/10.1016/j.pce.2016.05.001, 3rd International Conference on Ecohydrology, Soil and Climate Change, EcoHCC'14, 2016.

Castro-Camilo, D. and Huser, R.: Local Likelihood Estimation of Complex Tail Dependence Structures, Applied to U.S. Precipitation Extremes, J Am Stat Assoc, 115, 1037–1054, https://doi.org/10.1080/01621459.2019.1647842, 2020.

Ciais, P., Reichstein, M., Viovy, N., et al.: Europe-wide reduction in primary productivity caused by the heat and drought in 2003, Nature, 437, 529–533, https://doi.org/10.1038/nature03972, 2005.

Cinquini, L., Crichton, D., Mattmann, C., Harney, J., Shipman, G., Wang, F., Ananthakrishnan, R., Miller, N., Denvil, S., Morgan, M., Pobre, Z., Bell, G. M., Doutriaux, C., Drach, R., Williams, D., Kershaw, P., Pascoe, S., Gonzalez, E., Fiore, S., and Schweitzer, R.: The Earth System Grid Federation: An open infrastructure for access to distributed geospatial data, Future Gener Comp Sy, 36, 400–417, https://doi.org/https://doi.org/10.1016/j.future.2013.07.002, special Section: Intelligent Big Data Processing Special Section: Behavior

Data Security Issues in Network Information Propagation Special Section: Energy-efficiency in Large Distributed Computing Architectures Special Section: eScience Infrastructure and Applications, 2014.

Cleveland, R., Cleveland, W., McRae, J., and Terpenning, I.: STL: A seasonal-trend decomposition procedure based on loess, J Off Stat, 6, 3–33, 1990.

Coles, S., Pericchi, L. R., and Sisson, S.: A fully probabilistic approach to extreme rainfall modeling, J Hydrol, 273, 35 – 50, https://doi.org/10.1016/S0022-1694(02)00353-0, 2003.

Cooley, D., Naveau, P., and Poncet, P.: Variograms for spatial max-stable random fields, in: Dependence in Probability and Statistics, edited by Bertail, P., Soulier, P., and Doukhan, P., Springer, New York, 2006.

Danek, C., Shi, X., Stepanek, C., Yang, H., Barbi, D., Hegewald, J., and Lohmann, G.: AWI AWI-ESM1.1LR model output prepared for CMIP6 CMIP historical. Version 20200212, https://doi.org/10.22033/ESGF/CMIP6.9328, 2020.

de Bono, A., Giuliani, G., Kluser, S., and Peduzzi, P.: Impacts of summer 2003 heat wave in Europe, UNEP/DEWA/GRID European Environment Alertin Bulletin, 2, 1–4, 2004.

Dombry, C., Ribatet, M., and Stoev, S.: Probabilities of Concurrent Extremes, J Am Stat Assoc, 113, 1565–1582, https://doi.org/10.1080/01621459.2017.1356318, 2018.

Dong, B., Sutton, R. T., and Shaffrey, L.: Understanding the rapid summer warming and changes in temperature extremes since the mid-1990s over Western Europe, Clim Dynam, 48, 1537—-1554, https://doi.org/10.1007/s00382-016-3158-8, 2017.

EC-Earth Consortium: EC-Earth-Consortium EC-Earth3-Veg-LR model output prepared for CMIP6 CMIP historical. Version 20200217, https://doi.org/10.22033/ESGF/CMIP6.4707, 2020.

Eyring, V., Bony, S., Meehl, G. A., Senior, C. A., Stevens, B., Stouffer, R. J., and Taylor, K. E.: Overview of the Coupled Model Intercomparison Project Phase 6 (CMIP6) experimental design and organization, Geosci Model Dev, 9, 1937–1958, https://doi.org/10.5194/gmd-9-1937-2016, 2016.

Fischer, E. and Knutti, R.: Observed heavy precipitation increase confirms theory and early models, Nat Clim Change, 6, 986–991, https://doi.org/10.1038/nclimate3110, 2016.

Fisher, R. A. and Tippett, L. H. C.: Limiting forms of the frequency distribution of the largest or smallest member of a sample, Math Proc Cambridge, 24, 180—-190, https://doi.org/10.1017/S0305004100015681, 1928.

Fovell, R. G. and Fovell, M.-Y. C.: Climate zones of the Conterminous United States defined using cluster analysis, J Climate, 6, 2103 – 2135, https://doi.org/10.1175/1520-0442(1993)006<2103:CZOTCU>2.0.CO;2, 1993.

Fowler, H. J. and Kilsby, C. G.: Implications of changes in seasonal and annual extreme rainfall, Geophys Res Lett, 30, 2003.

Fréchet, M.: Sur la loi de probabilité de l'écart maximum, Ann Soc Polon Math, 6, 93–116, 1927.

Gnedenko, B.: Sur la distribution limite du terme maximum d'une série aléatoire, Ann Math, 44, 423–453, https://doi.org/10.2307/1968974, 1943.

Hagemann, S. and Dümenil, L.: A parametrization of the lateral waterflow for the global scale., Clim Dynam, 14, 17–31, 1997.

Harris, I., Osborn, T., Jones, P., et al.: Version 4 of the CRU TS monthly high-resolution gridded multivariate climate dataset, Scientific Data, 7, https://doi.org/10.1038/s41597-020-0453-3, 2020.

Horton, R., Mankin, J., Lesk, C., Coffel, E., and Raymond, C.: A review of recent advances in research on extreme heat events, Curr Clim Change Rep, 2, 242–259, https://doi.org/10.1007/s40641-016-0042-x, 2016.

Hosking, J.: Algorithm AS 215: Maximum-likelihood estimation of the parameters of the generalized extreme-value distribution, J Roy Stat Soc C-App, 34, 301–310, https://doi.org/10.2307/2347483, 1985.

Hosking, J., Wallis, J., and Wood, E.: Estimation of the generalized extreme-value distribution by the method of probability-weighted moments, Technometrics, 27, 251–261, https://doi.org/10.1080/00401706.1985.10488049, 1985.

Ionita, M., Caldarescu, D. E., and Nagavciuc, V.: Compound Hot and Dry Events in Europe: Variability and Large-Scale Drivers, Frontiers in Climate, 3, 58, https://doi.org/10.3389/fclim.2021.688991, 2021a.

Ionita, M., Dima, M., Nagavciuc, V., and Lohmann, G.: Past megadroughts in central Europe were longer, more severe and less warm than modern droughts, Communications Earth and Environment, 2, https://doi.org/10.1038/s43247-021-00130-w, 2021b.

IPCC: Managing the risks of extreme events and disasters to advance climate change adaptation. A special report of working groups I and II of the Intergovernmental Panel on Climate Change, Cambridge University Press, Cambridge, UK, and New York, NY, USA, https://doi.org/10.13140/2.1.3117.9529, 2012.

Jongman, B., Hochrainer-Stigler, S., Feyen, L., Aerts, J., Mechler, R., Botzen, W., Bouwer, L., Pflug, G., Rojas, R., and Ward, P.: Increasing stress on disaster-risk finance due to large floods, Nat Clim Change, 4, 264–268, https://doi.org/10.1038/NCLIMATE2124, 2014.

Kageyama, M., Harrison, S. P., Kapsch, M.-L., Lofverstrom, M., Lora, J. M., Mikolajewicz, U., Sherriff-Tadano, S., Vadsaria, T., Abe-Ouchi, A., Bouttes, N., Chandan, D., Gregoire, L. J., Ivanovic, R. F., Izumi, K., LeGrande, A. N., Lhardy, F., Lohmann, G., Morozova, P. A., Ohgaito, R., Paul, A., Peltier, W. R., Poulsen, C. J., Quiquet, A., Roche, D. M., Shi, X., Tierney, J. E., Valdes, P. J., Volodin, E., and Zhu, J.: The PMIP4 Last Glacial Maximum experiments: preliminary results and comparison with the PMIP3 simulations, Clim Past, 17, 1065–1089, https://doi.org/10.5194/cp-17-1065-2021, 2021a.

Kageyama, M., Sime, L. C., Sicard, M., Guarino, M.-V., de Vernal, A., Stein, R., Schroeder, D., Malmierca-Vallet, I., Abe-Ouchi, A., Bitz, C., Braconnot, P., Brady, E. C., Cao, J., Chamberlain, M. A., Feltham, D., Guo, C., LeGrande, A. N., Lohmann, G., Meissner, K. J., Menviel, L., Morozova, P., Nisancioglu, K. H., Otto-Bliesner, B. L., O'ishi, R., Ramos Buarque, S., Salas y Melia, D., Sherriff-Tadano, S., Stroeve, J., Shi, X., Sun, B., Tomas, R. A., Volodin, E., Yeung, N. K. H., Zhang, Q., Zhang, Z., Zheng, W., and Ziehn, T.: A multi-model CMIP6-PMIP4 study of Arctic sea ice at 127 ka: sea ice data compilation and model differences, Clim Past, 17, 37–62, https://doi.org/10.5194/cp-17-37-2021, 2021b.

Katz, R. and Brown, B.: Extreme events in a changing climate: Variability is more important than averages, Climatic Change, 21, 289–302, https://doi.org/10.1007/BF00139728, 1992.

Keeble, J., Hassler, B., Banerjee, A., Checa-Garcia, R., Chiodo, G., Davis, S., Eyring, V., Griffiths, P. T., Morgenstern, O., Nowack, P., Zeng, G., Zhang, J., Bodeker, G., Burrows, S., Cameron-Smith, P., Cugnet, D., Danek, C., Deushi, M., Horowitz, L. W., Kubin, A., Li, L., Lohmann, G., Michou, M., Mills, M. J., Nabat, P., Olivié, D., Park, S., Seland, Ø., Stoll, J., Wieners, K.-H., and Wu, T.: Evaluating stratospheric ozone and water vapour changes in CMIP6 models from 1850 to 2100, Atmos Chem and Phys, 21, 5015–5061, https://doi.org/10.5194/acp-21-5015-2021, 2021.

Kim, Y.-H., Min, S.-K., Zhang, X., Sillmann, J., and Sandstad, M.: Evaluation of the CMIP6 multi-model ensemble for climate extreme indices, Weather and Climate Extremes, 29, 100 269, https://doi.org/https://doi.org/10.1016/j.wace.2020.100269, 2020.

Kiriliouk, A., Rootzén, H., Segers, J., and Wadsworth, J. L.: Peaks Over Thresholds Modeling With Multivariate Generalized Pareto Distributions, Technometrics, 61, 123–135, https://doi.org/10.1080/00401706.2018.1462738, 2019.

Kornhuber, K., Coumou, D., Vogel, E., Lesk, C., Donges, J. F., Lehmann, J., and Horton, R.: Amplified Rossby waves enhance risk of concurrent heatwaves in major breadbasket regions, Nat Clim Change, 10, 48–53, https://doi.org/10.1038/s41558-019-0637-z, 2020.

Kovats, R. S. and Kristie, L. E.: Heatwaves and public health in Europe, Eur J Public Health, 16, 592–599, https://doi.org/10.1093/eurpub/ckl049, 2006.

Lohmann, G.: ESD Ideas: The stochastic climate model shows that underestimated Holocene trends and variability represent two sides of the same coin, Earth Syst Dynam, 9, 1279–1281, https://doi.org/10.5194/esd-9-1279-2018, 2018.

Lohmann, G., Butzin, M., Eissner, N., Shi, X., and Stepanek, C.: Abrupt Climate and Weather Changes Across Time Scales, Paleoceanography and Paleoclimatology, 35, e2019PA003 782, https://doi.org/https://doi.org/10.1029/2019PA003782, 2020.

Mahajan, S., Evans, K., Branstetter, M., Anantharaj, V., and Leifeld, J.: Fidelity of Precipitation Extremes in High Resolution Global Climate Simulations, Procedia Comput Sci, 51, 2178–2187, https://doi.org/10.1016/j.procs.2015.05.492, 2015.

Marcon, G., Padoan, S., Naveau, P., and Muliere, P.: Multivariate nonparametric estimation of the Pickands Dependence Function using Bernstein Polynomials, J Stat Plan Infer, 183, https://doi.org/10.1016/j.jspi.2016.10.004, 2014.

McNeil, A. J., Frey, R., and Embrechts, P.: Quantitative risk management: Concepts, techniques and tools. Revised edition, Economics Books, Princeton University Press, 2015.

Millard, S.: EnvStats, an R Package for Environmental Statistics. [Last access: 12 Feb 2021], https://cran.r-project.org/web/packages/EnvStats/index.html, 2013.

Mills, E.: Insurance in a climate of change, Science, 309, 1040–1044, https://doi.org/10.1126/science.1112121, 2005.

Mishra, V., Kumar, D., Ganguly, A. R., Sanjay, J., Mujumdar, M., Krishnan, R., and Shah, R. D.: Reliability of regional and global climate models to simulate precipitation extremes over India, J Geophys Res-Atmos, 119, 9301–9323, https://doi.org/https://doi.org/10.1002/2014JD021636, 2014.

Murtagh, F. and Contreras, P.: Algorithms for hierarchical clustering: an overview, WIREs Data Min Knowl, 2, 86–97, https://doi.org/10.1002/widm.53, 2012.

Myhre, G., Alterskjær, K., Stjern, C. W., et al.: Frequency of extreme precipitation increases extensively with event rareness under global warming, Sci Rep-UK, 9, https://doi.org/10.1038/s41598-019-52277-4, 2019.

Nazeri Tahroudi, M., Ramezani, Y., de Michele, C., and Mirabbasi, R.: Multivariate analysis of rainfall and its deficiency signatures using vine copulas, Int J Climatol, https://doi.org/https://doi.org/10.1002/joc.7349, 2021.

Neumann, A., Bodnar, T., Pfeifer, D., and Dickhaus, T.: Multivariate multiple test procedures based on nonparametric copula estimation, Biometrical J, 61, 40–61, https://doi.org/10.1002/bimj.201700205, 2019.

Niu, L., Lohmann, G., Gierz, P., Gowan, E. J., and Knorr, G.: Coupled climate-ice sheet modelling of MIS-13 reveals a sensitive Cordilleran Ice Sheet, Global Planet Change, 200, 103 474, https://doi.org/https://doi.org/10.1016/j.gloplacha.2021.103474, 2021.

Onwuegbuche, F., Kenyatta, A., Affognon, S. B., Enock, E., and Akinade, M.: Application of extreme value theory in predicting climate change induced extreme rainfall in Kenya, International Journal of Statistics and Probability, 8, https://doi.org/10.5539/ijsp.v8n4p85, 2019.

Opitz, T.: Extremal t-processes: Elliptical domain of attraction and a spectral representation, J Multivariate Anal, 122, 409—-413, https://doi.org/10.1016/j.jmva.2013.08.008, 2013.

Otto-Bliesner, B. L., Brady, E. C., Zhao, A., Brierley, C. M., Axford, Y., Capron, E., Govin, A., Hoffman, J. S., Isaacs, E., Kageyama, M., Scussolini, P., Tzedakis, P. C., Williams, C. J. R., Wolff, E., Abe-Ouchi, A., Braconnot, P., Ramos Buarque, S., Cao, J., de Vernal, A., Guarino, M. V., Guo, C., LeGrande, A. N., Lohmann, G., Meissner, K. J., Menviel, L., Morozova, P. A., Nisancioglu, K. H., O'ishi, R., Salas y Mélia, D., Shi, X., Sicard, M., Sime, L., Stepanek, C., Tomas, R., Volodin, E., Yeung, N. K. H., Zhang, Q., Zhang, Z., and Zheng, W.: Large-scale features of Last Interglacial climate: results from evaluating the *lig127k* simulations for the Coupled Model Intercomparison Project (CMIP6)–Paleoclimate Modeling Intercomparison Project (PMIP4), Climate of the Past, 17, 63–94, https://doi.org/10.5194/cp-17-63-2021, 2021.

570 Pickands, J.: Multivariate extreme value distributions, in: Proceedings of the 43rd Session of the International Statistical Institute, Vol. 2 (Buenos Aires, 1981), vol. 49, pp. 859–878, 894–902, International Statistical Institute, 1981.

Qian, L., Wang, H., Dang, S., Wang, C., Jiao, Z., and Zhao, Y.: Modelling bivariate extreme precipitation distribution for data-scarce regions using Gumbel–Hougaard copula with maximum entropy estimation, Hydrol Process, 32, 212–227, https://doi.org/10.1002/hyp.11406, 2018.

575 Rackow, T., Goessling, H., Jung, T., Sidorenko, D., Semmler, T., Barbi, D., and Handorf, D.: Towards multi-resolution global climate modeling with ECHAM6-FESOM. Part II: climate variability, Clim Dynam, 50, https://doi.org/10.1007/s00382-016-3192-6, 2018.

Rahmstorf, S. and Coumou, D.: Increase of extreme events in a warming world, P Natl Acad Sci USA, 108, 17 905–17 909, https://doi.org/10.1073/pnas.1101766108, 2011.

Reick, C. H., Raddatz, T., Brovkin, V., and Gayler, V.: Representation of natural and anthropogenic land cover change in MPI-ESM, J Adv
580 Model Earth Sy, 5, 459–482, https://doi.org/https://doi.org/10.1002/jame.20022, 2013.

Ribatet, M.: Modelling spatial extremes using max-stable processes, in: Nonlinear and Stochastic Climate Dynamics, edited by Franzke, C. L. E. and O'Kane, T. J., pp. 369–-391, Cambridge University Press, https://doi.org/10.1017/9781316339251.014, 2017.

Ribatet, M., Dombry, C., and Oesting, M.: Spatial extremes and max-stable processes, Extreme Value Modeling and Risk Analysis: Methods and Applications, pp. 179–194, https://doi.org/10.1201/b19721-10, 2015.

585 Salvador, S. and Chan, P.: Determining the number of clusters/segments in hierarchical clustering/segmentation algorithms, in: 16th IEEE International Conference on Tools with Artificial Intelligence, pp. 576–584, https://doi.org/10.1109/ICTAI.2004.50, 2004.

Schlather, M.: Models for stationary max-stable random fields, Extremes, 5, 33–44, https://doi.org/10.1023/A:1020977924878, 2002.

Schär, C., Vidale, P., Lüthi, D., Frei, C., Häberli, C., Liniger, M., and Appenzeller, C.: The role of increasing temperature variability in European summer heatwaves, Nature, 427, 332–336, https://doi.org/10.1038/nature02300, 2004.

590 Shaby, B. A. and Reich, B. J.: Bayesian spatial extreme value analysis to assess the changing risk of concurrent high temperatures across large portions of European cropland, Environmetrics, 23, 638–648, https://doi.org/https://doi.org/10.1002/env.2178, 2012.

Shi, X., Lohmann, G., Sidorenko, D., and Yang, H.: Early-Holocene simulations using different forcings and resolutions in AWI-ESM, The Holocene, 30, 996–1015, https://doi.org/10.1177/0959683620908634, 2020.

Sidorenko, D., Rackow, T., Jung, T., et al.: Towards multi-resolution global climate modeling with ECHAM6-FESOM. Part I: Model formu-
595 lation and mean climate, Clim Dynam, 44, 757–-780, https://doi.org/10.1007/s00382-014-2290-6, 2015.

Sillmann, J., Kharin, V. V., Zwiers, F. W., Zhang, X., and Bronaugh, D.: Climate extremes indices in the CMIP5 multimodel ensemble: Part 2. Future climate projections, J Geophys Res-Atmos, 118, 2473–2493, https://doi.org/https://doi.org/10.1002/jgrd.50188, 2013.

Smith, R. L.: Max-stable processes and spatial extremes, Unpublished Manuscript, 1990.

Stevens, B., Giorgetta, M., Esch, M., et al.: Atmospheric component of the MPI-M Earth System Model: ECHAM6, J Adv Model Earth Sy,
600 5, 146–172, https://doi.org/10.1002/jame.20015, 2013.

Tabari, H., De Troch, R., Giot, O., Hamdi, R., Termonia, P., Saeed, S., Brisson, E., Van Lipzig, N., and Willems, P.: Local impact analysis of climate change on precipitation extremes: are high-resolution climate models needed for realistic simulations?, Hydrol Earth Syst Sc, 20, 3843–3857, https://doi.org/10.5194/hess-20-3843-2016, 2016.

Tapiador, F. J., Turk, F., Petersen, W., et al.: Global precipitation measurement: Methods, datasets and applications, Atmos Res, 104-105,
605 70–97, https://doi.org/https://doi.org/10.1016/j.atmosres.2011.10.021, 2012.

Timmermans, B., Wehner, M., Cooley, D., O'Brien, T., and Krishnan, H.: An evaluation of the consistency of extremes in gridded precipita-
tion data sets, Clim Dynam, 52, 1–20, https://doi.org/10.1007/s00382-018-4537-0, 2019.

Toreti, A., Cronie, O., and Zampieri, M.: Concurrent climate extremes in the key wheat producing regions of the world, Sci Rep-UK, 9, https://doi.org/10.1038/s41598-019-41932-5, 2019.

610 Trenberth, K. E. and Fasullo, J. T.: An apparent hiatus in global warming?, Earths Future, 1, 19–32, https://doi.org/10.1002/2013EF000165, 2013.

University of East Anglia Climatic Research Unit, Harris, I. C., Jones, P. D., and Osborn, T.: CRU TS4.04: Climatic Research Unit (CRU) Time-Series (TS) version 4.04 of high-resolution gridded data of month-by-month variation in climate (Jan. 1901- Dec. 2019)., Centre for Environmental Data Analysis [data set], https://catalogue.ceda.ac.uk/uuid/89e1e34ec3554dc98594a5732622bce9, 2020.

615 Vandentorren, S., Suzan, F., Medina, S., Pascal, M., Maulpoix, A., Cohen, J.-C., and Ledrans, M.: Mortality in 13 French cities during the August 2003 heat wave, Am J Public Health, 94, 1518–20, https://doi.org/10.2105/AJPH.94.9.1518, 2004.

Vernieuwe, H., Vandenberghe, S., De Baets, B., and Verhoest, N. E. C.: A continuous rainfall model based on vine copulas, Hydrol Earth Syst Sc, 19, 2685–2699, https://doi.org/10.5194/hess-19-2685-2015, 2015.

Villarini, G., Smith, J. A., Ntelekos, A. A., and Schwarz, U.: Annual maximum and peaks-over-threshold analyses of daily rainfall accumu-
620 lations for Austria, J Geophys Res-Atmos, 116, https://doi.org/10.1029/2010JD015038, 2011.

Wang, Q., Danilov, S., Sidorenko, D., Timmermann, R., Wekerle, C., Wang, X., Jung, T., and Schröter, J.: The Finite Element Sea Ice-Ocean Model (FESOM) v.1.4: formulation of an ocean general circulation model, Geosci Model Dev, 7, 663–693, https://doi.org/10.5194/gmd-7-663-2014, 2014.

Weigel, K., Bock, L., Gier, B. K., Lauer, A., Righi, M., Schlund, M., Adeniyi, K., Andela, B., Arnone, E., Berg, P., Caron, L.-P., Cionni,
625 I., Corti, S., Drost, N., Hunter, A., Lledó, L., Mohr, C. W., Paçal, A., Pérez-Zanón, N., Predoi, V., Sandstad, M., Sillmann, J., Sterl, A., Vegas-Regidor, J., von Hardenberg, J., and Eyring, V.: Earth System Model Evaluation Tool (ESMValTool) v2.0 – diagnostics for extreme events, regional and impact evaluation, and analysis of Earth system models in CMIP, Geoscientific Model Development, 14, 3159–3184, https://doi.org/10.5194/gmd-14-3159-2021, 2021.

Zhang, Q., Li, J., Singh, V. P., and Xu, C.-Y.: Copula-based spatio-temporal patterns of precipitation extremes in China, Int J Climatol, 33,
630 1140–1152, https://doi.org/https://doi.org/10.1002/joc.3499, 2013.

Zhang, X., Alexander, L., Hegerl, G. C., Jones, P., Tank, A. K., Peterson, T. C., Trewin, B., and Zwiers, F. W.: Indices for monitoring changes in extremes based on daily temperature and precipitation data, WIREs Clim Change, 2, 851–870, https://doi.org/https://doi.org/10.1002/wcc.147, 2011.

Zscheischler, J., Mahecha, M. D., and Harmeling, S.: Climate classifications: the value of unsupervised clustering, Procedia Comput Sci,
635 9, 897–906, https://doi.org/10.1016/j.procs.2012.04.096, proceedings of the International Conference on Computational Science, ICCS 2012, 2012.

Zscheischler, J., Michalak, A. M., Schwalm, C., et al.: Impact of large-scale climate extremes on biospheric carbon fluxes: An intercomparison based on MsTMIP data, Global Biogeochem Cy, 28, 585–600, https://doi.org/https://doi.org/10.1002/2014GB004826, 2014.